Journal of
Materials Chemistry A

RSC Publishing

FEATURE ARTICLE

View Article Online
View Journal

$LiMnPO_4$ – A next generation cathode material for lithium-ion batteries

Cite this: DOI: 10.1039/c2ta01393b

Vanchiappan Aravindan,*[a] Joe Gnanaraj,*[b] Yun-Sung Lee*[c] and Srinivasan Madhavi*[ad]

Development of an eco-friendly, low cost and high energy density (~700 W h kg^{-1}) $LiMnPO_4$ cathode material became attractive due to its high operating voltage ~4.1 V *vs.* Li falling within the electrochemical stability window of conventional electrolyte solutions and offers more safety features due to the presence of a strong P–O covalent bond. The vacancy formation energy for $LiMnPO_4$ was 0.19 eV higher than that for $LiFePO_4$, resulting in a 10^{-3} times-diluted complex concentration, which represents the main difference between the kinetics in the initial stage of charging of two olivine materials. This review highlights the overview of current research activities on $LiMnPO_4$ cathodes in both native and substituted forms along with carbon coating synthesized by various synthetic techniques. Further, carbon coated $LiMnPO_4$ was also prepared by a solid-state approach and the obtained results are compared with previous literature values. The challenges and the need for further research to realize the full performance of $LiMnPO_4$ cathodes are described in detail.

Received 6th December 2012
Accepted 6th December 2012

DOI: 10.1039/c2ta01393b

www.rsc.org/MaterialsA

[a]*Energy Research Institute @ NTU (ERI@N), Nanyang Technological University, Research Techno Plaza, 50 Nanyang Drive, Singapore 637553, Singapore. E-mail: aravind_van@yahoo.com*

[b]*Yardney Technical Products, Inc., 82 Mechanic Street, Pawcatuck, CT 06379, USA. E-mail: joe@yardney.com*

[c]*Faculty of Applied Chemical Engineering, Chonnam National University, Gwang-ju 500-757, Korea. E-mail: leeys@chonnam.ac.kr*

[d]*School of Materials Science and Engineering, Nanyang Technological University, Singapore 639798, Singapore. E-mail: Madhavi@ntu.edu.sg*

Vanchiappan Aravindan is currently working in Energy Research Institute @ NTU (ERI@N), Nanyang Technological University, Singapore. He received his Ph.D. in 2009 from Gandhigram Rural University, Gandhigram, Tamilnadu, India. Then, he joined as a Post-Doctoral Fellow at The Research Institute for Catalysis, Chonnam National University, Gwang-ju, South Korea with Prof. Yun-Sung Lee, Faculty of Applied Chemical Engineering. Later, he moved in 2010 to the present organization to continue his research career. He has authored and co-authored over 70 peer-reviewed international publications and is currently serving as a reviewer for various international journals in the areas of electrochemistry and materials science. His research interests are in the development of high performance electrode and electrolyte materials for aqueous and non-aqueous Li-ion batteries and supercapacitors. He may be reached at aravind_van@yahoo.com.

Joseph Gnanaraj is a Senior Scientist at Yardney Technical Products Inc., Pawcatuck, CT. He received his M.Phil. from Bharathidasan University in 1990 and his research work was carried out at the Central Electrochemical Research Institute, Karaikudi, India, under the guidance of Dr Kuppusamy. He received Ph.D. in 1998 in Materials Science and Electrochemistry from University of Pune working with Prof. R.N. Karekar. He joined in 1999 as a Post-Doctoral Fellow and then in 2001 as a Senior Researcher with Professor Doron Aurbach, at Bar-Ilan University, Israel. He joined Worcester Polytechnic Institute, MA, in 2003 as a Visiting Research Scientist. He has authored and co-authored over 70 peer-reviewed international publications and is an active member of the Electrochemical Society Inc. He is a manuscript reviewer for various international journals of electrochemistry and materials. His research interests are in the fields of Li-ion batteries, electrode materials, organic electrolytes and hybrid Li-ion/ultra-capacitor systems. He may be reached at joe@yardney.com.

1 Introduction

Despite a few drawbacks like poor shelf life and a small risk of fire, lithium-ion batteries (LIBs) still remain a popular as well as a portable electrochemical energy storage device in this era. The LIB power packs are intensively pursued for electric (EV), hybrid electric (HEV) and plug-in electric vehicle (P-HEV) applications.[1–12] This is because of lithium having a very small atomic mass (6.94 g mol^{-1}), thereby reducing the weight of the battery drastically. Combined with this fact, lithium is extremely reactive, so it can give off a tremendous amount of energy in its chemical reactions with a theoretical capacity of 3862 A h kg^{-1} and higher potential (−3.05 V *vs.* normal hydrogen electrode) and these factors influence a very high energy density of the cell. Briefly, LIBs offer a very meager amount of self-discharge (∼5% per month), no memory effect, high energy density (both volumetric and gravimetric), *etc.*[5,13–17] The characteristics of three generations of LIBs are compared with other commonly available rechargeable systems, like lead acid, Ni–MH, Ni–Cd and magnesium, in Table 1.[18]

Practically, metallic lithium based rechargeable batteries were first demonstrated by Whittingham[19] in the 1970's using TiS_2 as the cathode and lithium as the anode with a limited cell potential (<2.5 V *vs.* Li). The pioneering work of Goodenough and co-workers[20–22] invented the possibility of using layered $LiCoO_2$ and spinel $LiMn_2O_4$ as cathode materials for lithium rechargeable cells in the 1980's with an extended cell voltage of above 4 V *vs.* Li. Further, the demonstration of reversible lithium insertion into graphite by Yazami and Touzain[23] followed by the successful development of carbonaceous anodes by Sony Inc. led to the successful commercialization of LIBs in 1990. Thereafter, many materials such as $LiNiO_2$, $LiMnO_2$, V_2O_5, *etc.* were proposed as possible alternatives to the existing layered $LiCoO_2$ cathodes due to its own setbacks.[24–30] Also, Goodenough and co-workers[2,31–33] reported the utilization of polyanion framework materials as prospective cathodes for LIBs. Among them $LiFePO_4$ was found to be better and it was commercialized recently by A123 Inc., and Sony Inc., owing to its appealing properties like the presence of Fe which is environmentally benign, low cost, very stable electrochemical properties with structural stability, high thermal stability and a long distinct discharge plateau. The comparison among the cathode materials is schematically illustrated in Fig. 1.[34] Most of the LIBs are used in portable electronic devices such as laptops, cell phones and portable electronic devices fabricated with layered oxides as cathodes and carbonaceous materials as anodes. The inherent toxicity, chemical instability and high cost along with safety issues occurring during high voltage charge (>4.3 V *vs.* Li) arising from a significant overlap of the $Co^{3+/4+}$:3d band with the top of the O_2^-:2p bands hinder the possible usage of cobalt-rich cathodes in heavier configurations like HEV and P-HEV applications.[35]

From the cost and environmental points of view, cathodes based on transition metal elements like Mn and Fe would be beneficial. In that scenario, the spinel $LiMn_2O_4$ is attractive, as Mn is inexpensive and eco-friendly. Its three-dimensional structure with a good structural stability supports high rate capability which is one of the prerequisites for the above-mentioned EV based applications. However, $LiMn_2O_4$ suffers from severe capacity fade at elevated temperatures due to the dissolution of Mn^{3+} from the spinel lattice and the consequent attack of carbonaceous anodes by the solvated Mn atoms, resulting in an increase in cell impedance.[4] On the other hand, in recent years significant progress, such as surface modification with inactive particles, carbon coating, and partial replacement of isovalent or aliovalent cations, *etc.*, has been

Yun-Sung Lee is currently working as Associate Professor at Chonnam National University, Gwang-ju, South Korea. He received his M.S. from Chonbuk National University in 1998 and his research work was carried out under the guidance of Prof. Kee-Suk Nahm. He received his Ph.D. in 2001 in Applied Chemistry from Saga University in Japan under the direction of Prof. Masaki Yoshio. He joined in 2001 as a Post-Doctoral Fellow as a Doctoral Researcher with Professor Yuichi Sato, at Kanagawa University in Japan. He joined Chonnam National University in 2003 as Assistant Professor. He has authored and co-authored over 100 peer-reviewed international publications and is an active member of the lithium secondary battery field. His research interests are in the fields of Li-ion batteries, electrode materials, and hybrid capacitor systems. He may be reached at leeys@chonnam.ac.kr.

Madhavi Srinivasan is currently an Assistant Professor at the School of Materials Science and Engineering, Nanyang Technological University (NTU), Singapore. She graduated from Indian Institute of Technology (IIT), Chennai (India), and completed her Ph.D. from National University of Singapore (Singapore). Her research interest lies in enhancing performance of energy storage devices such as lithium ion batteries, supercapacitors and advanced batteries with the help of multifunctional nanoscale materials to power printed electronics, store energy from renewable sources and for powering electric vehicles. Her focus is on fabrication and investigation of nanoscale materials/architectures for electrochemical energy storage devices. She may be contacted at Madhavi@ntu.edu.sg.

Table 1 A comparison among the rechargeable battery systems[18]

	Magnesium	Lead acid	Ni–Cd	Ni–MH	Li-ion I	Li-ion II	Li-ion III
Anode	Mg alloy	Pb	Cd	$MH(LaNi_5H_6)$	LiC_6	Sn–Co–C–Ti	LiC_6
Cathode	Mo_3S_4	PbO_2	NiOOH	NiOOH	$LiCoO_2$	$LiCoO_2$ + $Li(Ni–Co–Mn)O_2$	$LiFePO_4$
Electrolyte	$Mg(AlCl_2BuEt)$ in THF/TG	Aqueous H_2SO_4	Aqueous KOH	Aqueous KOH	$LiPF_6$[a]	$LiPF_6$[a]	$LiPF_6$[a]
Specific energy density (theory) (W h kg^{-1})	135	170	220	220	410	226	560
Specific energy density (practical)(W h kg^{-1})	>60	30–40	40–60	75–100	120–150	158	95
Working voltage (V)	1.3–1.0	2.0–1.8	1.2–1.0	1.2–1.0	4.0–3.0	4.2–2.5	3.6–2.0
Working temperature (°C)	−20 to +80	−20 to +50	−40 to +45	−20 to +45	−30 to +80	−30 to +80	−30 to +80
Chemical overcharge protection	No	Yes	Yes	Yes	No[b]	No[b]	No[c]
Chemical overdischarge protection	No	No	Yes	Yes	No[b]	No[b]	No[b]
Cycle number, 100% DOD	>2000	>50	>1000	>1000	<1000	<1000	>3000
Relative toxicity	Low?	High	High	High	Medium	High	Low
Safety	High?	High	High	High	Medium	Medium	High
Estimated material costs	Low	Medium	Medium	Medium-high	High	Medium	Medium
Estimated manufacture cost	High	Low	Medium	Medium	High	High	High

[a] Salt in aprotic organic solvents or polymers, DOD – depth of discharge. [b] Electronic control of the state of charge/discharge. [c] A123 uses redox shuttle mechanisms through additives, TG – tetraglyme.

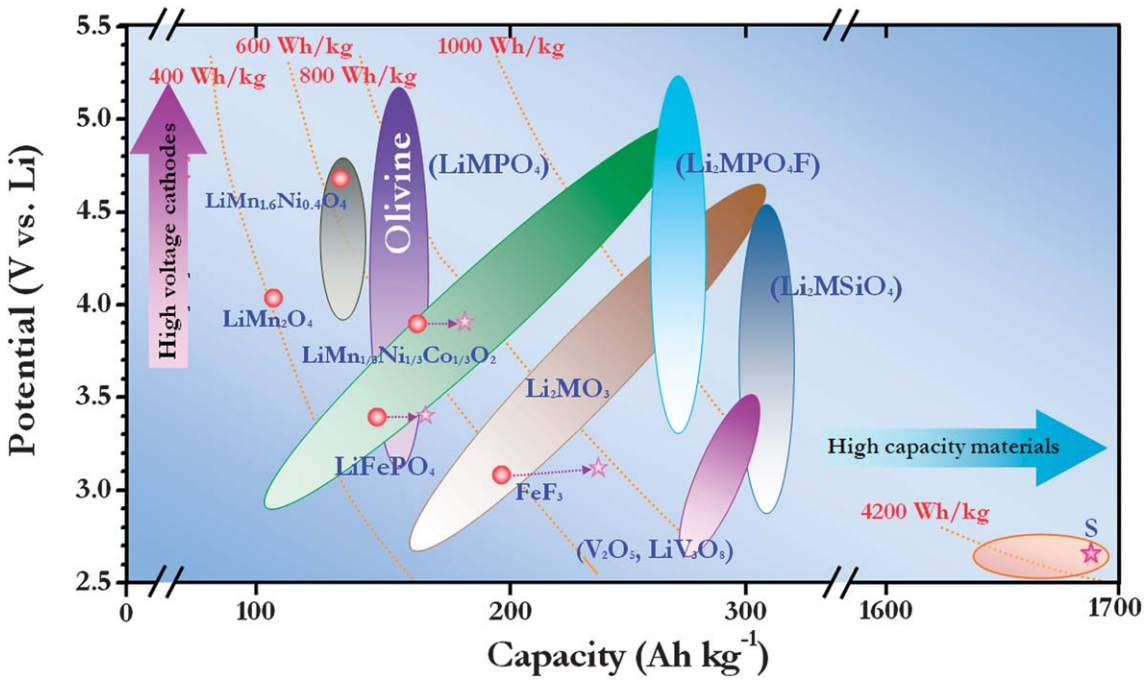

Fig. 1 Schematic representation of the plot of Li-ion battery cathode material potentials *vs.* capacity. $LiMPO_4$, Li_2MSiO_4 and Li_2MPO_4F, where M = Fe, Mn, Co, Ni, *etc.*; Li_2MO_3, where M = Mn, Mo, Ir, Ru, *etc.*[34]

made to retain $LiMn_2O_4$ as a serious contender for high power applications.[36,37] A partial substitution of Mn atoms provides the possibility of using them as 5 V (*vs.* Li) cathodes in LIBs. The simple oxides such as $LiCoO_2$, $LiNiO_2$, and $LiMn_2O_4$ with highly oxidized redox couples ($Co^{3+/4+}$, $Ni^{3+/4+}$ and $Mn^{3+/4+}$) were able to offer high cell potentials in LIBs.[38,39] Nevertheless, operation of such materials at elevated temperatures could lead to the release of oxygen from the lattice in the charged state due to the

lack of chemical stability of highly oxidized species such as Co^{4+} and Ni^{4+}, which results in the thermal runway of the cell.[40] One way to overcome this problem is to work with lower-valence redox couples like $Fe^{2+/3+}$. However, a decrease in the oxidation state will raise the redox energy of the cathode and lower the cell voltage. Keeping this in mind, Goodenough and co-workers[2,41–47] focused on the development of polyanion framework materials, which comprise oxygen in tetrahedral sites, for example XO_4^{2-} (X = S, Mo, and W). The polyanion-containing $Fe_2(SO_4)_3$ host was found to operate at 3.6 V *vs.* Li while both $Fe_2(MoO_4)_3$ and $Fe_2(WO_4)_3$ were found to operate at 3.0 V *vs.* Li. The aforementioned Fe based hosts have NASICON-related framework structures, in which the FeO_6 octahedra share corners with XO_4 tetrahedra resulting in Fe–O–X–O–Fe linkages. The lack of direct Fe–Fe or Fe–O–Fe interaction results in inherent electronic conductivity and low rate capability despite good lithium ion conduction in such NASICON-based frameworks.[44,46,48,49]

With their continuous efforts, in 1997 Goodenough and co-workers[33] discovered the olivine type $LiFePO_4$ as the host matrix for Li-ion insertion and extraction. Initial results suggest that insertion and extraction of 0.6 moles of lithium were feasible and excellent reversibility with a distinct plateau around ~3.4 V *vs.* Li was exhibited. $LiFePO_4$ comprising an orthorhombic unit cell (D_{2h}^{16} space group *Pmnb*), which accommodates four units of $LiFePO_4$, and the oxygen ions form a hexagonal close-packed arrangement. The Fe ions form zigzag chains of octahedra in alternate basal planes bridged by the tetrahedral phosphate units (PO_4). Li atoms occupy the octahedral sites, which are located in the remaining basal planes, and Li^+ ions form one dimensional tunnels in the structure that run parallel to the planes of corner-sharing FeO_6 octahedra, along the [010] direction in the orthorhombic *Pmnb* lattice. The strong covalent bond between oxygen and P^{5+} ions forming $(PO_4)^{3-}$ units allows greater stabilization of the structure when compared to other counterparts like $LiCoO_2$, $LiNiO_2$ and $LiMn_2O_4$. Furthermore, strong covalence stabilizes the anti-bonding $Fe^{3+/2+}$ state through a Fe–O–P inductive effect. As a result, it is very difficult to remove oxygen atoms from the lattice due to the tetrahedral arrangement. This structure provides high thermal stability for elevated temperature operations. This P_{tet}–O–Fe_{oct} linkage in the structure generates a suitable $Fe^{3+/2+}$ redox energy of flat voltage 3.4 V *vs.* Li. At the same time, $LiFePO_4$ was severely affected by poor electronic conductivity issues ($\sim10^{-9}$ S cm^{-1}) because of the separated arrangement of FeO_6 octahedra.[35] The carbon coating, creating rich or deficient sites of lithium and partial substitution of either isovalent or aliovalent cations significantly improved the conductivity thereby enabling better battery performance and approaching the theoretical capacity (~170 mA h g^{-1}). Even though commercialization of C–$LiFePO_4$ nanocomposites was achieved by one US venture company (A123 Inc.) for power tool applications, Sony announced the mass production of $LiFePO_4$ based batteries into the market for EV applications. However, the energy densities (~578 W h kg^{-1}) of such cells are limited due to the restricted operating potential ~3.4 V *vs.* Li, which is quite low for high power applications such as EV and HEV.[50] Thus, research is devoted to the development of other members of olivine phosphates group unveiling similar properties to $LiFePO_4$, such as $LiMnPO_4$, $LiCoPO_4$ and $LiNiPO_4$.[51–53] Among the members of the above olivine family, the latter two exhibited redox reactions at ~4.8 and ~5.2 V *vs.* Li, respectively, which are higher than the safer operational limit of conventional carbonate based electrolyte solutions. Thus, the current research is devoted to develop eco-friendly, low cost $LiMnPO_4$ with a high operating voltage ~4.1 V *vs.* Li and capable of delivering a maximum energy density of ~700 W h kg^{-1} with more safety features due to the presence of a strong P–O covalent bond. More importantly, the electrochemical window falls within the electrochemical stability window of conventional electrolyte solutions, when compared to other systems.[54] Nevertheless, only very few researchers have realized the full performance of $LiMnPO_4$ in the native form. In this paper, we describe an overview of current research activities on $LiMnPO_4$ with our experimental results in detail.

1.1 Solid-state approach

After the successful extraction and reversible insertion of Li-ions into polyanion type $LiFePO_4$ by Padhi *et al.*,[33,45] the same approach was attempted to extract Li-ions from the $LiMnPO_4$ matrix in the presence of 1 M $LiClO_4$ in propylene carbonate (PC) and dimethoxyethane (DME) solution. However, the authors failed to extract Li-ions from the native compound, whereas Fe doping on Mn sites leads to the extraction of Li-ions and oxidation of Mn^{2+} was observed after the oxidation of Fe^{2+}. The prominent voltage plateaus of Fe and Mn were located at ~3.4 and 4.1 V *vs.* Li, when Mn concentration exceeds 50% ($x \geq 0.5$) ($LiMn_{1-x}FePO_4$). A maximum of ~0.45 moles Li per formula unit were only extracted for a Mn content of 75%. When the concentration of Fe substitution is increased (beyond 50%) Li-ion extraction tends to decrease. In order to complement Padhi *et al.*[33] work, Okada *et al.*[55] also attempted to extract lithium from the native compound when charged up to 5.2 V *vs.* Li in the presence of 1 M $LiPF_6$ in an ethylene carbonate (EC) : dimethyl carbonate (DMC) solution but failed in their attempt. Yamada *et al.*[56] pointed out that smooth extraction of lithium from the native compound was too complicated because of its insulating behaviour, when compared to semiconductor type $LiFePO_4$ and Jahn–Teller (JT) deformation around Mn^{3+} was also a major factor responsible for such huge polarization during the electrochemical reaction. Further, the electrochemical performance of $LiMnPO_4$ is entirely different from its counterpart $LiFePO_4$. The current durability for Li_xMnPO_4 is orders-of-magnitude inferior to that for Li_xFePO_4, and its origin was clearly attributed to the intrinsic crystallographic and transport properties of Li_xMnPO_4. Moreover, $LiMnPO_4$ is an insulator with a ~2 eV spin exchange band gap, whereas $LiFePO_4$ is a semiconductor with a ~0.3 eV crystal field band gap. Heavy polaronic holes localized on the Mn^{3+} sites were suggested as an important rate-limiting factor. For example, in order to achieve an energy density as large as that of $LiFePO_4$, only less than one tenth of the current can be allowed to pass through $LiMnPO_4$. More simply, $LiMnPO_4$ exceeds the energy density of $LiFePO_4$ at the 10 day rate, and it reaches its theoretical energy density at the 1 month

discharge rate. The electrochemical cycling process has been described by Goodenough's core–shell two phase reaction model.[33] In spite of the higher open-circuit voltage of $Mn^{3+/2+}$ (~4.05 V *vs.* Li) compared to that of $Fe^{3+/2+}$ (~3.4 V *vs.* Li) in the olivine framework, the abnormally large polarization may eliminate pure $LiMnPO_4$ as a practical lithium battery cathode due to much lower effective energy density than $LiFePO_4$. Further, the sophisticated synthetic recipe may somewhat improve the reaction kinetics; there should always be large relative kinetic differences coming from the intrinsic properties dominating the overall trend.

The JT effect associated with Mn^{3+} was also reported by Nie *et al.*[57] *via* first principles calculations. A large volume change (~6.5%) during transition from $LiMnPO_4$ (316.41 Å) to $MnPO_4$ (296.20 Å) was noticed due to extraction of lithium. The migration energy barrier of those JT-type small polarons was related to the energy levels of the Mn-3 d($x^2 - y^2$) states above the Fermi level, while the energy level of those Mn-3 d($x^2 - y^2$) states determines the energy gap. Based on the above, the predicted band gaps of 3.96, 1.07 and 0.27 eV were calculated for $LiMnPO_4$, $MnPO_4$ and $Li_{0.5}MnPO_4$ phases, respectively. As there were no Mn^{2+} in ideal $MnPO_4$ lattices and no Mn^{3+} in ideal $LiMnPO_4$ lattices, the migration of polarons was restricted by concentration of defects (such as Li vacancies in $LiMnPO_4$ and Li-ions in $MnPO_4$) in real cases. Thus, the electrical conduction in $MnPO_4$ and $LiMnPO_4$ was poor as compared to that of $Li_{0.5}MnPO_4$. Hence although the JT effect was harmful to the structural stability, it was helpful for electrical conduction in Li_xMnPO_4. Further, Asari *et al.*[58] theoretically investigated the formation and diffusion of a vacancy–polaron complex in $LiMnPO_4$ and $LiFePO_4$ using the first-principles density functional theory (DFT) within a framework of the GGA + U method. The vacancy formation energy for $LiMnPO_4$ was 0.19 eV higher than that for $LiFePO_4$, resulting in a 10^{-3} times-diluted complex concentration, which represents the main difference between the kinetics in the initial stage of charging of two olivine materials. This large difference was caused by insufficient relaxation of Mn–O bonds in $LiMnPO_4$.

Later in 2002, Li *et al.*[59] successfully demonstrated extraction and reversible insertion of Li-ions from C–$LiMnPO_4$ composite cathodes, in which cathodes comprising 9.8 wt% carbon were prepared *via* a solid state route followed by ball milling with carbon. The test cells were cycled between 2 and 4.5 V at 0.28 mA cm^{-2} in the presence of 1 M $LiPF_6$ in EC : DMC. During charging to 4.5 V *vs.* Li by CC mode, a capacity of 162 mA h g^{-1} was observed which corresponds to the extraction of 0.94 Li per formula unit. The cell delivered a first discharge capacity of 146 mA h g^{-1} and a stable reversible capacity of ~140 mA h g^{-1} was noted in subsequent cycles. The authors also tried to charge the cell up to 4.8 V *vs.* Li for complete removal of Li-ions from the lattice. In that situation, the first charge capacity approaches the theoretical value (~171 mA h g^{-1}); nevertheless only 0.89 moles of lithium (152 mA h g^{-1}) reversibly inserted during the subsequent discharge. Moreover, severe capacity fading was observed during cycling. Li *et al.*[59] explained that the cause for such a fade was mainly due to the decomposition of the electrolyte used. In $LiMnPO_4$, only 10.7% of volume change was noticed during extraction and insertion of Li-ions (cell volume 302.9 $Å^3$ for $LiMnPO_4$ and 270.4 $Å^3$ for Li_0MnPO_4) based on the two phase model suggested by Padhi *et al.*[33] DSC was also conducted to study the thermal stability in the de-lithiated state of Li_xMnPO_4 and heat evolution of 290 J g^{-1} was determined, which indicates good thermal stability when compared to other layered type cathodes like $LiCoO_2$ (1000 J g^{-1}) and $LiNiO_2$ (1600 J g^{-1}). This confirms the strong P–O bonding influence in olivine phase materials which renders high temperature tolerance.

Kang and co-workers[60–62] also investigated the thermal properties of lithiated and de-lithiated phases of Li_xMnPO_4. During de-lithiation, a colour change from white to purple was noted and the two phase reaction was confirmed by continuous XRD measurements. The morphology of the above phases was severely influenced by phase transition. It is surprising to note that de-lithiated $MnPO_4$ was extremely unstable, even during exposure to the electron beam while recording the TEM images. At the same time, de-lithiated Li_xMnPO_4 was thermally stable at elevated temperatures (up to 410 °C) and no structural changes were noted. However, raising the temperature leads to an increase in unit cell volume and lattice parameters. At relatively low temperatures, only $LiMnPO_4$ and $MnPO_4$ co-exist; upon heating, $MnPO_4$ partially decomposes into $Mn_2P_2O_7$ and O_2 is released according to the following equation

$$2MnPO_4 \rightarrow Mn_2P_2O_7 + \frac{1}{2}O_2$$

It is well known that oxygen extraction from the P–O covalent bond is too difficult, and olivine-type materials are therefore considered as thermally safer electrodes for LIBs. It is worthy to mention that O_2 evolution can readily occur through decomposition at a temperature as low as 210 °C in the presence of an electrolyte solution. The irreversible phase transformation of the de-lithiated phase, if it occurs, deteriorates the electrochemical performance of a $LiMnPO_4$ electrode. According to Delacourt *et al.*[63] PO_4^{3-} anion was thermally stable up to ~500 °C and was evaluated in various compositions of $Li_{1-x}FePO_4$ and other polyanion type electrodes. A similar kind of thermal

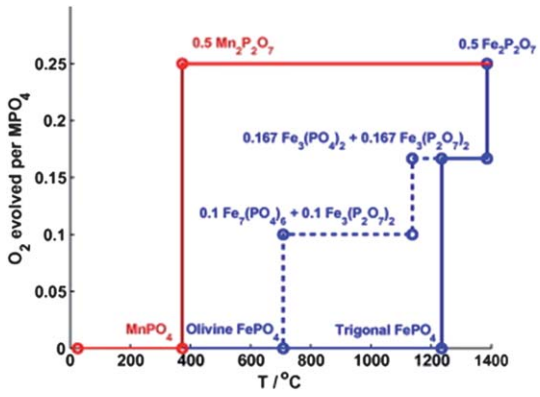

Fig. 2 O_2 evolved *versus* temperature for de-lithiated MPO_4 (M = Fe and Mn).[65] Copyright: Elsevier

instability was also noticed by Chen and Richardson[64] and Ong *et al.*,[65] and they pointed out that manganese may also have a catalytic effect on the decomposition of the phosphate to release oxygen rather than its counterpart $LiFePO_4$.

In contrast to the above reports, recently Aurbach and co-workers[66] found that the thermal stability of $LiMnPO_4$ and solid-solution $LiMn_{0.8}Fe_{0.2}PO_4$ was not inferior when compared to $LiFePO_4$. The exothermal reactivity (specific heat evolution) of de-lithiated olivine phase materials was found to follow the order, $Li_{0.1}MnPO_4$ > $Li_{0.05}Mn_{0.8}Fe_{0.2}PO_4$ > $Li_{0.05}FePO_4$ while using 1 M $LiPF_6$ in EC : DMC as the electrolyte, whereas the above trend was reversed while using 1 M $LiPF_6$ in EC : PC. Further, it is worthy to mention that $LiMPO_4$ (M = Fe and Mn) olivine phase materials did not release oxygen upon heating which reflects better structural stability than that of the layered type cathodes. Further, no noticeable change in the XRD patterns of de-lithiated olivine cathodes before and after heating to 400 °C was observed. As indicated by TGA measurements, heating to such high temperatures leads to the reaction between Li_xMPO_4 and the carbon coating which may be accompanied by the formation of new phases. These results clearly indicate that the three fully de-lithiated olivine phases were basically stable at high temperatures, *i.e.* up to 400 °C, and it was consistent with the simulation by Ong *et al.*[67] using first principles calculations and this is illustrated in Fig. 2. Conversely, other cathodes like $LiCoO_2$ and $LiNi_{0.8}Co_{0.15}Al_{0.05}O_2$ in the de-lithiated state demonstrated noticeable structural changes upon heating to 400 °C. This confirmed the superior thermal stability of $LiMPO_4$ compounds in the de-lithiated state. The obtained results have been confirmed by thermogravimetric analysis coupled with mass spectroscopic measurements (TGA-MS). Moreover, the authors clearly stated that the scientific community has not yet reached the same level of understanding and comprehension of $LiMnPO_4$ that exists to date with $LiFePO_4$. Further, it may not be surprising that different batches of $LiMnPO_4$ synthesized in different ways behave very differently in terms of both electrochemical performance and thermal stability. Hence, it is too early to derive general conclusions about the safety features of Li_xMnPO_4 as a cathode material for Li-ion batteries. To support the explanation given by Aurbach and co-workers,[66] Choi *et al.*[68] extensively studied the thermal stability and structural change using *in situ* hot stage X-ray diffraction measurements and compared with $MnPO_4 \cdot H_2O$ powder. The results clearly suggested that de-lithiated $MnPO_4$ undergoes a structural change to form the $Mn_2P_2O_7$ phase at 490 °C with subsequent evolution of O_2 according to the above equilibrium and this reaction was coinciding with the structural change observed in $MnPO_4 \cdot H_2O$ powders.

Shiratsuchi *et al.*[69] adopted the isovalent and aliovalent doping (Ti, Mg and Zr) on Mn sites to improve the electrochemical properties of $LiMnPO_4$. After the preparation of the $LiMn_{1-x}M_xPO_4$ (where M = Ti, Mg and Zr) phase, the compound was mixed with 25 wt% of acetylene black and milled using a planetary ball miller with subsequent heat treatment. During the treatment, the authors noticed the occurrence of carbothermal reduction to form the Mn_2P phase for the first time in $LiMnPO_4$ while the final sintering temperature exceeds

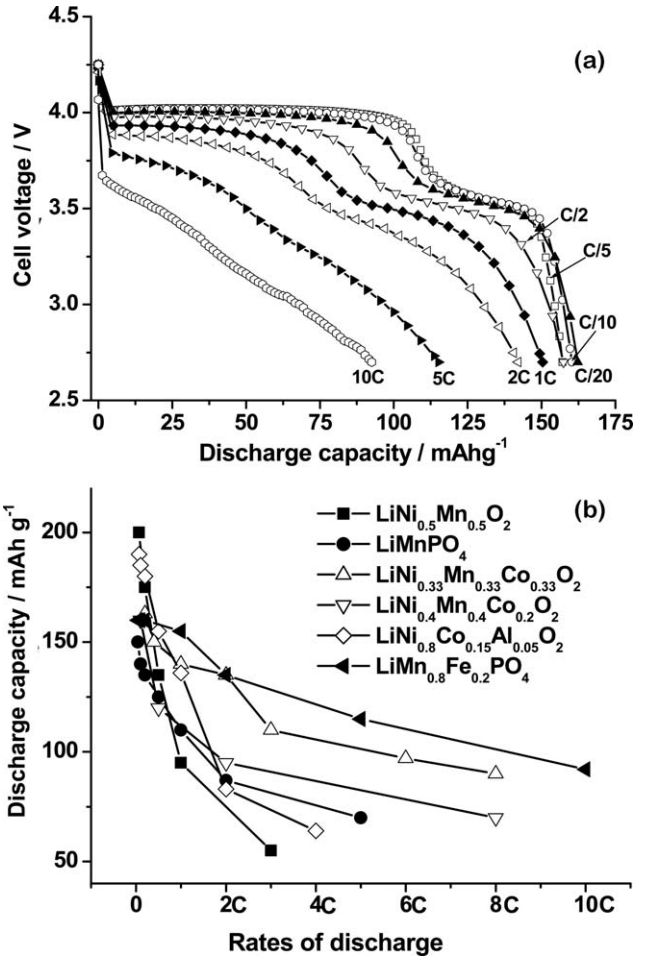

Fig. 3 (a) Typical voltage profiles of C–$LiMn_{0.8}Fe_{0.2}PO_4$ composite electrodes measured galvanostatically at various discharge rates at 30 °C in the standard electrolyte solution. The term C rate describes the rate of discharge, whereby a constant current is chosen so that the entire maximal specific capacity (165 mA h g^{-1}) is discharged during a specified period of time; for example, the rate 0.1 C means that the constant current is adjusted to discharge the entire capacity during 10 h, and at rates 1 or 2 C the entire capacity is discharged within 1 or 0.5 h, respectively. (b) Comparison of rate capabilities (discharge capacity *versus* discharge rate) for C–$LiMn_{0.8}Fe_{0.2}PO_4$, C–$LiMnPO_4$, $LiNi_{0.33}Mn_{0.33}Co_{0.33}O_2$, $LiNi_{0.4}Mn_{0.4}Co_{0.2}O_2$, $LiNi_{0.5}Mn_{0.5}O_2$, and $LiNi_{0.8}Co_{0.15}Al_{0.05}O_2$ (NCA) cathodes in similar experiments (galvanostatic cycling at 30 °C in standard electrolyte solutions). The potential windows within which C–$LiMn_{0.8}Fe_{0.2}PO_4$, C–$LiMnPO_4$, and the layered transition-metal-oxide cathodes reached their full capacity were 2.7–4.25, 2.7–4.4, and 2.5–4.5 V *versus* Li.[71] Copyright: John Wiley & Sons, Inc.

600 °C. Hence, an optimized annealing temperature was required to avoid the formation of Mn_2P. In Mn site doping, an improvement of one order of electronic conductivity was noted for all the doped olivine phase materials ($LiMnPO_4 \sim 10^{-11}$ S cm^{-1}, for $LiMn_{0.99}Ti_{0.01}PO_4$, $LiMn_{0.99}Mg_{0.01}PO_4$, and $LiMn_{0.99}Zr_{0.01}PO_4 \sim 10^{-10}$ S cm^{-1}) at room temperature. The Mg-doped (1%) sample displayed better rate capability and was found to be the most effective dopant for $LiMnPO_4$ when compared to rest of the two ions used for this study. Specifically, the discharge capacity of the 1% Mg-doped sample was ~136 mA h g^{-1} at 1.0 mA cm^{-2} and ~125 mA h g^{-1} at a higher current of 2.0 mA cm^{-2}. These values are 10 and 20% larger than those

of Zr doped and native compounds, respectively, whereas in $LiFePO_4$ the rate capability was drastically enhanced by 1% Zr doping by Chung *et al.*[70] Unfortunately, Zr doping was not effective for $LiMnPO_4$ to improve its performance.

The effect of Fe^{2+} substitution was also successfully employed by Martha *et al.*[71] to form a solid-solution between olivine phases of Fe and Mn. A solid-state method was employed for the preparation of such a $LiMn_{0.8}Fe_{0.2}PO_4$ phase along with 10 wt% carbon followed by ball milling before the heat treatment at 550 °C for 3 h in Ar atm. The olivine phase $LiMn_{0.8}Fe_{0.2}PO_4$ comprised 25–60 nm size particulates with ~5 nm thick carbon coating on the surface. It was surprising to notice that the reactivity of the $LiMn_{0.8}Fe_{0.2}PO_4$ phase towards electrolyte solutions was much lower than the native phases of either $LiMnPO_4$ or $LiFePO_4$ observed through ac impedance measurements. Similar to the above-mentioned synthesis, C–$LiMnPO_4$ was prepared by a polyol process;[72] $LiMn_{0.8}Fe_{0.2}PO_4$ displayed excellent rate performance above the 2 C rate compared to other counterparts like $LiNi_{0.33}Mn_{0.33}Co_{0.33}O_2$, $LiNi_{0.4}Mn_{0.4}Co_{0.2}O_2$, $LiNi_{0.5}Mn_{0.5}O_2$, and $LiNi_{0.8}Co_{0.15}Al_{0.05}O_2$, and even C–$LiMnPO_4$ (Fig. 3). The potential limits for these tests were determined between 2.5 and 4.25 V by a CC–CV protocol for olivine phase materials. An initial discharge capacity of 160–165 mA h g^{-1} (close to the theoretical value of 170 mA h g^{-1}) was observed at low rates (0.1 C). A negligible capacity fading was observed throughout the testing range with an extent of decay less than 0.025 mA h g^{-1} per cycle at a 1 C rate for about 300 cycles. The thermal stability of C–$LiMn_{0.8}Fe_{0.2}PO_4$ falls between C–$LiMnPO_4$ and C–$LiFePO_4$, whereas the thermal stability of de-lithiated C–$Li_xMn_{0.8}Fe_{0.2}PO_4$ is higher than that of de-lithiated C–Li_xMnPO_4 and C–Li_xFePO_4 in terms of both the onset temperatures of the main thermal reactions and the specific heat evolution. Further, the authors also first demonstrated the electrochemical performance of C–$LiMnPO_4$ and C–$LiMn_{0.8}Fe_{0.2}PO_4$ cathodes with the spinel $Li_4Ti_5O_{12}$ anode in a full cell configuration for load leveling applications.[73] Zou *et al.*[74] also reported the performance of C–$LiMn_{0.8}Fe_{0.2}PO_4$ by varying the carbon source (carbon clack and sucrose) and ball milling duration with $Li_4Ti_5O_{12}$ anodes.

Yang *et al.*[75] reported the synthesis of Co-doped $LiMnPO_4$ ($LiMn_{0.95}Co_{0.05}PO_4$) by an oleic acid assisted approach. The source materials were initially ball milled before the heat treatment in a N_2 atmosphere at various calcination temperatures. The sample prepared at 600 °C performed better when compared to other temperature conditions and it showed discharge capacities of 103 and 144 mA h g^{-1} for $LiMnPO_4$ and $LiMn_{0.95}Co_{0.05}PO_4$, respectively at a 0.05 C rate between 2.5 and 4.5 V using the CC–CV protocol. The capacity fading was observed in both cases of the materials prepared by this route. Further, it was apparent that Co^{2+} doping on Mn sites leads to a decrease in cell volume and the chemical diffusion co-efficient is also calculated through CV analysis and was found to be 3.0×10^{-17} cm^2 s^{-1}.

After the successful synthesis of $LiMnPO_4$ nanoplates by Wang *et al.*[72] *via* the polyol procedure, the same group of authors attempted isovalent (Mg, Fe, Zn and Ni) doping on Mn sites.[76] The doped and native compounds were prepared under an Ar–H_2 atm. and the prepared phase materials were subsequently ball milled with 20 wt% carbon. The capacity of C–$LiMn_{0.9}Fe_{0.1}PO_4$ was around 30% higher than native C–$LiMnPO_4$ for all the current rates tested by CC–CV mode. For example, C–$LiMn_{0.9}Fe_{0.1}PO_4$ showed ~148 mA h g^{-1} at 0.05 C, whereas the native compound exhibited only ~114 mA h g^{-1}. At 0.2 C, the values were found to be 123 and 90 mA h g^{-1}, respectively. C–$LiMn_{0.9}M_{0.1}PO_4$ (M = Mg and Ni) exhibits a similar performance to C–$LiMnPO_4$ at 0.2, 0.5 and 1 C rates while discharge capacities were slightly higher. As far as zinc-substitution was concerned, it exhibits a poor behavior, only 77 mA h g^{-1} at 0.05 C, compared to other substituents. Electronic conductivity was only slightly improved with dopants (Fe, Ni and Mg) and this was in contrast to $LiFePO_4$ where electronic conductivity was drastically enhanced. For example, electronic conductivity of $LiMnPO_4$ is 1.02×10^{-9} S cm^{-1}, around 1/3 of the Fe modified (2.85×10^{-9} S cm^{-1}), and 8.4 times of $LiMn_{0.9}Zn_{0.1}PO_4$ (1.21×10^{-10} S cm^{-1}).

Lee *et al.*[77] investigated various ranges of cation substitutions (Mg^{2+}, Ca^{2+} and Zr^{4+}) under N_2 flow at 600 °C for about 3 h. It is obvious that there was no appreciable variation in the unit cell volume during cationic substitution. However, as far as the electrochemical performance was concerned, substitution of Mg^{2+} and Zr^{4+} resulted in decrease in polarization and increase in capacity profile. For example, Mg^{2+} doped $LiMnPO_4$ delivered a discharge capacity of ~120 mA h g^{-1} between 2 and 4.5 V at 7.5 mA g^{-1}, when compared to ~90 mA h g^{-1} for native $LiMnPO_4$ by the CC–CV protocol. The authors also found that co-doping of Zr^{4+} along with Mg^{2+} ($LiMn_{0.88}Mg_{0.1}Zr_{0.02}PO_4$) provides further decrease in polarization (~177 mV for $LiMn_{0.9}Mg_{0.1}PO_4$ and ~153 mV for $LiMn_{0.88}Mg_{0.1}Zr_{0.02}PO_4$) of the electrodes. In the case of Ca^{2+} substitution, the performance was very poor compared to that of the native compound. Chemical diffusivity of Zr^{4+} co-doped phases was one order of magnitude higher than that of the $LiMnPO_4$ phase (8.8×10^{-15} to 2.9×10^{-14} cm^2 s^{-1}) and an improved capacity retention of 83% (initial discharge capacity ~125 mA h g^{-1}) was maintained at 30 mA g^{-1}, whereas only 68% capacity (initial discharge capacity ~85 mA h g^{-1}) was retained for pristine $LiMnPO_4$.

$LiMnPO_4$ with an off-stoichiometry ($LiMn_{0.9}P_{0.95}O_{4-\delta}$) was reported by Kang and Ceder[78] with a particle size of <50 nm. The prepared phase contains some impurity phases like Li_3PO_4 and $Li_4P_2O_7$; the concentration of those phases was totally less than 5% of the native compound, hence the theoretical capacity of $LiMnPO_4$ was assumed to be 162 mA h g^{-1}. The test cell showed a discharge capacity of ~145 mA h g^{-1} between 3 and 4.8 V at 0.05 C which is ~89% of theoretical capacity, whereas the native compound showed a discharge capacity of 80 mA h g^{-1} by CC mode. At a high current rate (1 C), $LiMn_{0.9}P_{0.95}O_{4-\delta}$ delivered a capacity of ~65 mA h g^{-1} and it is twice that of the nominal composition. The authors attempted to increase the carbon content (65 wt%) during the formulation of the electrodes, nevertheless no significant improvement was achieved.

A molten hydrocarbon assisted solid-state procedure has been adopted to synthesize nano-platelets of $LiMnPO_4$ by a single step process.[79] The $LiMnPO_4$ nanoplates show identical orientation with preferred growth on the order of [010] > [001] > [100] with

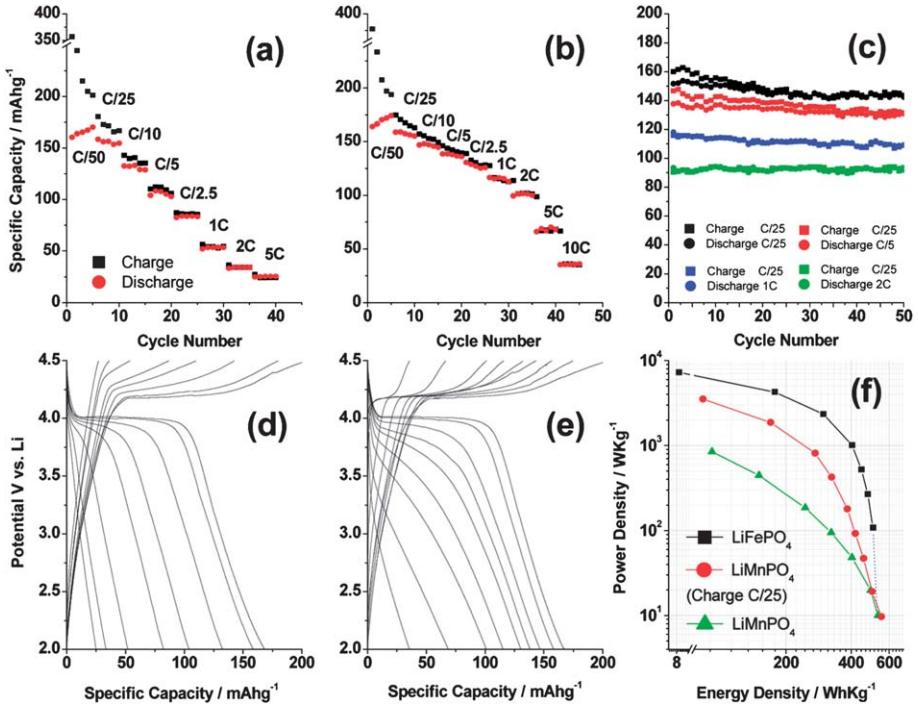

Fig. 4 Rate performance of $LiMnPO_4$ during (a) same charge–discharge C-rates and (b) various discharge C-rates following a constant charge at 0.04 C and (c) extended electrochemical cycling on cells after rate evaluations. Voltage–capacity profiles of $LiMnPO_4$ nanoplates cycled at (d) the same charge–discharge C-rates, (e) various discharge C-rates following a constant charge at 0.04 C, and (f) Ragone plot comparison of $LiMnPO_4$ and $LiFePO_4$.[79] Copyright: American Chemical Society.

[010] and [001] being very close. However, thinner platelets were grown along the *a*-axis [100], which is not a favorable direction for Li-ion diffusion. On the other hand, the [010] growth was more favorable for a cathode material because a flat potential is guaranteed by the two-phase transition during the electrochemical Li insertion/extraction process. Carbon coating was also performed by using a planetary ball milling procedure with 20 wt% of carbon. After the milling process, the platelet morphology was still maintained and a huge increase in specific surface area was also noted ($\sim$157 $m^2\ g^{-1}$), whereas the crystallite size reduced from $\sim$27 to $\sim$24 nm. The cycling performances were conducted in CC mode between 2 and 4.5 V *vs.* Li at room temperature and a specific discharge capacity of 168 mA h g^{-1} was achieved at 0.02 C, which is close to the theoretical capacity. The electrochemical cycling profiles of the $LiMnPO_4$ nanoplates are given in Fig. 4.

To prepare Fe and Mg co-doped $LiMnPO_4$ with 14 wt% of sucrose, a solid-state route has been adopted with subsequent ball milling for 6 h by Hu *et al.*[80,81] Four different synthesis temperatures namely, 650, 750, 800 and 850 °C were studied. When the temperature exceeds 800 °C it leads to the formation of Fe_2P impurity during Fe substitution. Hence, 800 °C for 10 h was well suited to obtain the best performing single phase material. The final product comprised $\sim$7.5 wt% carbon for all the three temperatures, except 850 °C ($\sim$5.7 wt%). Since the ionic radii of Mg^{2+} (0.66 Å) and Fe^{2+} (0.74 Å) are smaller than that of Mn^{2+} (0.80 Å), the substitution clearly results in a crystal lattice shrink and a subsequent cell volume decrease. The electrochemical properties of C–$LiMn_{0.9}Fe_{0.1-x}Mg_xPO_4$, where $x = 0.01$, 0.02 and 0.05, were evaluated using CC–CV mode at 4.5 V *vs.* Li. Capacity profiles increased with increasing synthesis temperature and it could be attributed to the increased electronic conductivity of the carbon film, *i.e.* graphitization and improved crystallinity of the $LiMn_{0.9}Fe_{0.05}Mg_{0.05}PO_4$ phase achieved by high temperature sintering. It is clear that $LiMn_{0.9}Fe_{0.05}Mg_{0.05}PO_4$ powder delivered a much higher reversible capacity as compared to the $LiMnPO_4$ and $LiMn_{0.9}Fe_{0.1}PO_4$ phases. The initial discharge capacity at 0.2 C was 67 mA h g^{-1} for pure $LiMnPO_4$, 74 mA h g^{-1} for $LiMn_{0.9}Fe_{0.1}PO_4$, and 121 mA h g^{-1} for $LiMn_{0.9}Fe_{0.05}Mg_{0.05}PO_4$. The rate performance of $LiMn_{0.9}Fe_{0.05}Mg_{0.05}PO_4$ displayed a reversible capacity of 140 mA h g^{-1} at 0.1 C, 117 mA h g^{-1} at 1 C, 103 mA h g^{-1} at 2 C, 90 mA h g^{-1} at 3 C and 62 mA h g^{-1} at 5 C.

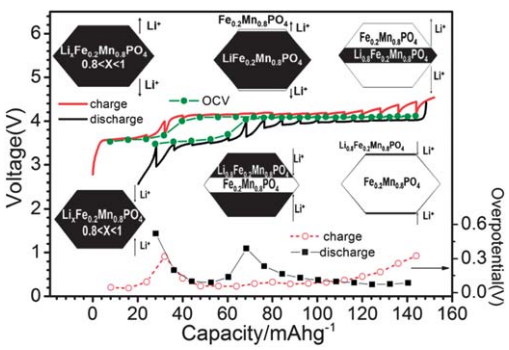

Fig. 5 GITT profile, open-circuit voltage curves, and overpotential curves of the carbon-coated mesoporous $LiFe_{0.2}Mn_{0.8}PO_4$ cell during charge and discharge. Inset: scheme of the electrochemical reaction.[84] Copyright: The Electrochemical Society.

Zn doping on Mn sites was reported by Wang *et al.*,[82] in which β-cyclodextrin was used as the source material for carbon with a fixed 1 : 5 weight ratio with $LiMnPO_4$. A maximum specific discharge capacity of ~140 mA h g^{-1} was obtained for C–$LiMn_{0.95}Zn_{0.05}PO_4$ at a 0.02 C rate between 2.4 and 4.5 V by CC mode when compared to C–$LiMnPO_4$ (~70 mA h g^{-1}). The composite electrode, C–$LiMn_{0.95}Zn_{0.05}PO_4$ delivers discharge capacities of ~120 and ~111 mA h g^{-1} at 0.05 and 0.1 C rates, respectively under room temperature conditions. Further, it is worthy to mention that Zn doping enables the reduction in polarization of the electrode.

Hong *et al.*[83] reported a Fe substituted olivine phase, $LiMn_{1-x}Fe_xPO_4$ ($x = 0$, 0.05, 0.1, 0.15, and 0.2) prepared with an appropriate amount of citric acid as the carbon source and subsequently employed planetary ball milling for about 3.5 days before the heat treatment. All the prepared samples showed similar diffraction patterns, except for a slight shift towards higher angles with increasing concentration of Fe ions and the unit cell shrank continuously as iron was introduced into the system. The cell experienced a discharge capacity of ~133 and ~138 mA h g^{-1} at 0.1 C between 2.8 and 4.4 V by CC mode for 15 and 20% of Fe concentration, and those cells presented a solid-solution behavior when the Fe concentration exceeded 10% when compared to the native compound (55 mA h g^{-1} at 0.067 C).

Carbon coated mesoporous $LiFe_{0.2}Mn_{0.8}PO_4$ was reported by Zhang *et al.*[84] using citric acid and sucrose as the source materials for carbon and followed by ball milling before heat treatment. After the ball milling procedure, a surface area of 57 m^2 g^{-1} was noted for the above-mentioned compound. Mesoporous $LiFe_{0.2}Mn_{0.8}PO_4$ exhibited good reversible capacities of 140 and 120 mA h g^{-1} for 0.05 and 0.1 C, respectively between 2.6 and 4.5 V by CC mode. The obtained capacity is better than the non-porous one, which delivers a reversible capacity of 120 and 80 mA h g^{-1} under the same test conditions. The GITT measurements reveal the two-phase behavior of the $Mn^{3+/2+}$ redox couple and the solid-solution behavior of the $Fe^{3+/2+}$ region, which are clearly given in Fig. 5.

Muraliganth and Manthiram[85] reported the solid-solution between $LiMnPO_4$ and either $LiCoPO_4$ or $LiFePO_4$ by a high energy ball milling procedure with 20 wt% carbon in the final product. The discharge capacity increases significantly from 91 mA h g^{-1} in $LiMnPO_4$ to 142 mA h g^{-1} in $LiMn_{0.75}Fe_{0.25}PO_4$, and 155 mA h g^{-1} for $LiMn_{0.5}Fe_{0.5}PO_4$ at 0.05 C, whereas $LiCoPO_4$ and $LiMnPO_4$ solid-solutions experienced severe capacity fade due to the poor compatibility of the electrolyte. The GITT measurements confirm the sluggish kinetic behavior of $LiMnPO_4$ and this was partly due to the large volume expansion (8.9%) during the phase transition from $LiMnPO_4$ to $MnPO_4$ and the intrinsic nature of the native phase as well.

1.2 Sol–gel technique

Ethylene glycol assisted synthesis of $LiMPO_4$ (M = Fe, Mn and Co) nanostructures were reported by Yang and Xu[86] to enable *in situ* carbon coating. *In situ* carbon coating over $LiMnPO_4$ particles by using organic precursors was successful and it was found that 3.3 wt% of carbon was covered on the surface after the phase formation at 700 °C in a N_2 atmosphere. The Li/$LiMnPO_4$ cell was cycled between 2.5 and 4.5 V in CC mode and delivered a reversible capacity of 85 and 42 mA h g^{-1} at 0.01 and 0.05 C rates, respectively. Moreover, the presence of such a carbon layer enables reversible insertion of Li-ion around 4.1 V *vs.* Li with the two-phase behaviour. Kwon *et al.*[87] successfully synthesized nanosized (140–130 nm) $LiMnPO_4$ particles by a glycolic acid assisted sol–gel approach. The prepared $LiMnPO_4$ was ball milled with 20 wt% carbon for size reduction as well as to enable carbon coating. The cycling profiles indicate reduction of particle size from 830 to 140 nm which resulted in improved electrochemical performance (~134 mA h g^{-1} for 140 nm particles) between 2.3 and 4.5 V at 0.1 C. At 1 C, 140 nm particulates exhibited a reversible capacity of ~81 mA h g^{-1}, whereas 270 nm particles showed a reversible capacity of ~5 mA h g^{-1} only. The authors pointed out that improvement in both ionic and electronic conductivity is required for the improved performance of the electrode. The improvement of ion transport was achieved by reducing the particle size and ensuring narrow size distribution. An increase in electron transport can be achieved by adopting carbon coating.

The effect of particle size on the electrochemical behavior of carbon coated $LiMnPO_4$ was reported by Drezen *et al.*[88] utilizing the conventional sol–gel technique followed by dry ball milling with 20% carbon. During the synthesis, increasing the calcination temperature led to the formation of nanometer to submicrometer particles. This size variation strongly influenced the electrochemical activity during Li-ion insertion/extraction, for example 140, 160, 200, 270 and 830 nm size particles exhibited a discharge capacity of 134, 120, 100, 90 and 60 mA h g^{-1} respectively, at 0.1 C rate at room temperature by CC mode. It is obvious that as the particle size increases, lithium diffusion becomes progressively difficult due to both diffusion limitation of Li^+ within a single large particle and complex pathways for electron transport through the bulk. When the primary particle size is large, it will take a much longer time for lithium ions to diffuse into the core of the particle to make a single homogeneous phase from $LiMn^{2+}PO_4$ to $Mn^{3+}PO_4$ ideally.

A liquid phase synthesis was also reported by Doi *et al.* to reduce the particle size in the presence of long chain oleic acids comprising 18 atoms of carbon.[89] For this synthesis, the total reaction was completed at less than 300 °C resulting in the formation of $LiMnPO_4$. The obtained compound delivered a discharge capacity of 6 mA h g^{-1} between 3 and 4.5 V at 0.01 C by CC mode. After heat treatment at 500 °C for 1 h in Ar, the long chain oleic acid was burned and converted to carbon. The shape of the rods with a length of 100–250 nm and width of 40–125 nm was retained, even after carbonization. Moreover, $LiMnPO_4$ nanorods were covered well with carbon during such process. Carbonization results in improvement in the electrochemical properties of cells with a discharge capacity of 65 mA h g^{-1} at 0.01 C.

Isovalent and aliovalent doping (Mg^{2+}, Fe^{2+}, Co^{2+}, V^{3+} and Gd^{3+}) on Mn^{2+} sites was reported by Yang *et al.*[90] and such phases were prepared by a solution phase reaction using citric acid as the carbon source. The precursors were ball-milled for 10 h in a planetary ball miller and fired at 700 °C for 20 h in a N_2

atmosphere. The substitution in Mn sites ($LiMn_{0.95}M_{0.05}PO_4$, M = Mg, V, Fe, Co and Gd) clearly revealed the increase in unit cell volume for all cases, except for Fe^{2+}. The cell delivered a discharge capacity of 45, 61, 32, 102 and 59 mA h g^{-1} at room temperature (25 °C), and 113, 120, 95, 149 and 117 mA h g^{-1} at an elevated temperature (50 °C) for Mg, V, Fe, Co and Gd substitutions, respectively, between 2.7 and 4.4 V in CC–CV mode. A similar trend was also noticed while increasing the upper cut-off potential to 4.8 V in the same CC–CV mode. However, in all cases capacity fading was observed irrespective of the cut-off potentials and testing temperature.

In order to prevent the dissolution of Mn into the electrolyte solution, an ionic liquid based approach was utilized by Kim *et al.*[91] $LiMnPO_4$ was synthesized by a conventional citric acid assisted sol–gel process and the final product yielded 9.8 wt% carbon. 0.5 M LiTFSI in EMImTFSI solution was used as the lithium source trapped in a homemade electrospun membrane and it showed an ionic conductivity of 10^{-3} S cm^{-1} at 0 °C. The discharge capacity for the $LiMnPO_4$/ionic liquid based electrolyte cell was stable at ~120 mA h g^{-1} over 50 cycles. After 50 cycles, the conventional electrolyte (1 M $LiPF_6$ in EC : DMC) comprising cell retains ~56% of the initial discharge capacity whereas the ionic liquid based cell retains ~99%. The XPS study shows the absence of Mn 2p peaks, which indicates that Mn dissolution was found to be less than 0.1 wt% or 5 ppm after storage for 4 weeks in the ionic liquid medium.

Preparation of $LiMnPO_4$ composites with single walled carbon nanotubes (SWCNTs) was suggested by Weglikowska *et al.*[92] The authors intended to increase the surface area thereby achieving full performance of the material by utilizing a self-supported electrode or conventional coating technique. It is worth mentioning that addition of 1 wt% of SWCNTs contributes to the increase of the BET surface area of the resulting composite (SWCNT–$LiMnPO_4$). This indicates that the presence of SWCNTs during the formation of crystallites increases the number of nucleation sites and leads to a reduction in the size of the particle. Further, electrical conductivity can be improved by five orders of magnitude through *in situ* addition of 1 wt% of SWCNTs. Battery performance revealed that 68–83% of theoretical capacity can be achieved by using the buckypaper electrode at 0.1 C rate with a more or less single phase reaction.

Nithya *et al.*[93] reported the synthesis of $LiMn_{0.91}Co_{0.09}PO_4$ by a glycine assisted sol–gel approach with the particulate size ranging from 50 to 300 nm. The resultant phase was ball milled with the desired amount of carbon (acetylene black 30 wt%) to yield a high performance cathode. C–$LiCo_{0.09}Mn_{0.91}PO_4$ delivered a maximum discharge capacity of 162 mA h g^{-1} between 3 and 4.9 V *vs.* Li (CC mode) at 0.1 C when compared to 70, 140 and 148 mA h g^{-1} for $LiMnPO_4$, C–$LiMnPO_4$ and $LiCo_{0.09}Mn_{0.91}PO_4$, respectively. It is interesting to note that a very low amount of capacity fade and polarization (100 mV) of the electrode was noted during $Mn^{3+/2+}$ redox reactions.

1.3 Polyol procedure

A polyol mediated procedure was adopted to synthesize the high performance platelet shaped $LiMnPO_4$ nanostructures.[72] The poor intercalation of Li^+ ions due to Jahn–Teller (JT) distortion is well known and it was predicted to be unavoidable in Mn(III) [d_4: $t_{2g}^3e_g^1$] of $MnPO_4$. The prepared platelet morphology was oriented along the *a–c* plane, hence Li-ion moves parallel to *b*. As such, this unique platelet morphology was optimal for rapid ionic diffusion and good kinetics during lithium insertion and extraction in olivine framework materials. The prepared platelets were milled with 20% of carbon to form a C–$LiMnPO_4$ composite. The cell, Li/C–$LiMnPO_4$ delivered an initial discharge capacity of 145 and 141 mA h g^{-1} at 0.05 and 0.1 C rates, respectively, at room temperature. As expected, while increasing the temperature from ambient to 50 °C, the composite C–$LiMnPO_4$ approaches (159 mA h g^{-1}) 93% of theoretical capacity at 0.1 C rate. The durability of the composite was also evaluated; in the 199th cycle it displays 97% capacity of the 9th cycle (loss of only ~5 mA h g^{-1}) at ambient temperature. Interestingly, even better performance was noted in the elevated temperature (50 °C) operation and the total fading was estimated as only 9 mA h g^{-1} from the 1st to the 200th cycle at 0.1 C rate (CC–CV mode). Moreover, there was no increase in polarization of the electrode recorded throughout the testing. At 1 C, the cell retained a discharge capacity of 113 mA h g^{-1} (80%) at ambient temperature and 138 mA h g^{-1} (86%) at 50 °C. The authors claimed that the improved performance was due to the rigid three-dimensional structure which was stabilized by strong covalent bonds between oxygen and the phosphorus ions. In addition to that mentioned above, the nano-structure morphology of polyol mediated $LiMnPO_4$ enhanced its durability. Further, there has been much debate concerning the presence and function of Jahn–Teller distortion in $MnPO_4$. This implies that JT distortion plays a different role in $LiMnPO_4$, and may even stabilize the structure well. Moon *et al.*[94] continued the synthesis of $LiMnPO_4$ by the polyol process and carbon coating (20%) by high energy ball milling. However, lithium cyclability was found to be poor when compared to the

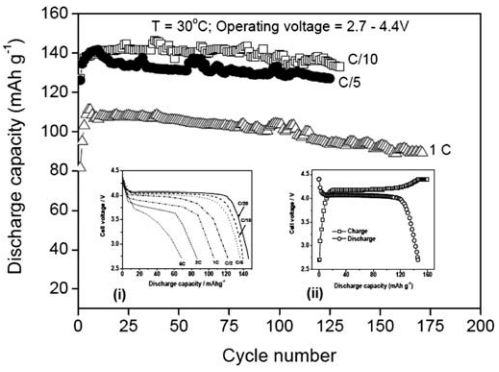

Fig. 6 Cycling behavior at various rates of discharge (as indicated) of composite electrodes comprising nanosized C–$LiMnPO_4$ particles in the potential range of 2.7–4.4 V in EC–DMC 1 : 2/$LiPF_6$ 1.5 M solutions (coin-type cell, T = 30 °C). The cycling protocol was CC–CV providing potentiostatic steps at 4.4 V during 5 h for 0.1 C rate, 2.5 h for 0.2 C rate, and 30 min for 1 C rate. Inset (i) shows voltage profiles of the C–$LiMnPO_4$ composite electrodes measured galvanostatically at various discharge rates (T = 30 °C) as indicated between 4.4 and 2.7 V *vs.* Li, and inset (ii) shows typical charge–discharge profiles of these C–$LiMnPO_4$ composite electrodes at 0.05 C rate.[97] Copyright: The Electrochemical Society.

previous work by Wang *et al.*[72]; for example, carbon-coated C–$LiMnPO_4$ exhibited a specific capacity of ~68 and ~52 mA h g^{-1} at 0.05 and 0.1 C rates, respectively when cycled between 2.7 and 4.4 V (CC–CV mode). Kim *et al.*[95] also reported the polyol mediated synthesis of $LiMnPO_4$ nanoplatelets, which showed a reversible capacity of 115 mA h g^{-1} at 0.1 mA cm^{-2} by CC mode. However, the Li/$LiMnPO_4$ cells did not show any noticeable plateau around 4.1 V *vs.* Li, though the electrodes were formulated with 35 wt% carbon.

After the demonstration of high performance composite C–$LiMnPO_4$ by High Power Lithium (HPL), Martha *et al.*[71,73,96,97] reported the surface features and comparative study with other conventional cathodes, such as $LiNi_{0.5}Mn_{0.5}O_2$, $LiNi_{0.33}Mn_{0.33}Co_{0.33}O_2$, $LiNi_{0.4}Mn_{0.4}Co_{0.2}O_2$ and $LiNi_{0.8}Co_{0.15}Al_{0.05}O_2$. The Li/C–$LiMnPO_4$ cell displays an initial discharge capacity of 145 mA h g^{-1} under ambient conditions as described by HPL and the corresponding charge–discharge curves are given in Fig. 6. The composite, C–$LiMnPO_4$ exhibited better rate capabilities (>2 C) than both $LiNi_{0.5}Mn_{0.5}O_2$ and $LiNi_{0.8}Co_{0.15}Al_{0.05}O_2$ electrodes. The voltage profiles of the all layered type nickel-based materials showed monotonous sloping curves because of the single phase reaction, while that of C–$LiMnPO_4$ was flat (due to the Li insertion into this material that involves a first-order phase transition). Surface chemical aspects of C–$LiMnPO_4$ were also addressed under three different conditions, namely, as prepared (C–$LiMnPO_4$), C–$LiMnPO_4$ aged for 3 weeks in 1.5 M $LiPF_6$ in EC : DMC (1 : 2 vol) solution at 30 °C and aged for 3 weeks in 1.5 M $LiPF_6$ in EC : DMC solution at 60 °C. The impedance spectra of aged C–$LiMnPO_4$ clearly exhibited well defined, semi-circular high-to-medium frequency features, and low frequency Warburg-type straight-line features, whereas pristine C–$LiMnPO_4$ showed only the 'Warburg tail'. Both aged C–$LiMnPO_4$ powders confirmed the increase in impedance during 3 weeks in the presence of the electrolyte solution. FT-IR studies showed that there was no appreciable variation in all the three powders tested. The XPS spectra of C 1s, P 2p, O 1s and Mn $2p_{3/2}$ regions indicated that there was no shift between the parent and aged C–$LiMnPO_4$. At the same time, the Li 1s region of these particles shows a slight change due to aging, *i.e.*, the appearance of a small peak around 56 eV and this can be attributed to the formation of LiF. LiF and additional species with C–F bonds are formed and precipitate on the particle's surface (covered with carbon) in standard solutions. Such a precipitation of surface species may well explain the increase in impedance during aging in solutions. LiF can be formed by the decomposition of $LiPF_6$ at relatively low temperatures and can be catalyzed by the particle surface. The dissolution studies showed that all Li, Mn and P ions were less soluble (0.015%) at 60 °C in the above electrolyte during aging for a seven week period and the dissolution range was meager when compared to $LiFePO_4$.[98] Both $LiMnPO_4$ and Li_xMnPO_4 undergo exothermal reactions with 1 M $LiPF_6$ in EC–DMC (1 : 1, vol) solutions in the 180–300 °C temperature range, as found for all other cathode materials. Nevertheless, the specific heat evolution from these thermal reactions of $LiMnPO_4$ was much lower compared to the heat evolution from the thermal reactions of $LiNi_{0.8}Co_{0.15}Al_{0.05}O_2$ and this result confirms the previous report by Li *et al.*[59] The improved thermal stability could be achieved by adopting carbon coating, which can impede direct and fast thermal reactions between solution species and the active mass at high temperatures. Kumar *et al.*[99] also tried the same procedure to obtain high performance $LiMnPO_4$ nanorods with carbon decoration using a resin coating process. Unfortunately, C–$LiMnPO_4$ did not show any prominent plateau around ~4.1 V *vs.* Li.

1.4 Spray pyrolysis

In the recent past, Taniguchi and co-workers[100–105] reported the synthesis of $LiMnPO_4$ by spray pyrolysis followed by wet ball milling with 10% acetylene black and ethanol to make the carbon composite. Finally, the composite was fired at 500 °C for 4 h in a N_2 + 3% H_2 environment and found that discharge capacity increases with the charge cut-off voltage. About 23% increase in the discharge capacity was observed while the upper cut-off voltage was increased from 4.4 (91 mA h g^{-1}) to 4.5 V (112 mA h g^{-1}), and 64% for a cut-off voltage increase from 4.4 to 4.9 V (149 mA h g^{-1}) at room temperature. The same kind of improvement was also noticed in CC–CV mode as well. The Li/C–$LiMnPO_4$ cell exhibits higher discharge capacities under CC mode rather than CC–CV mode, for example, 153, 149, 85 and 42 mA h g^{-1} at 0.05, 0.1, 1 and 5 C, respectively, whereas discharge capacities of 132, 120 and 91 mA h g^{-1} at 0.1, 1 and 5 C, respectively were observed in the latter mode. The influence of surface area on the electrochemical performance of $LiMnPO_4$ was also reported by the same authors by adjusting the firing temperature and increasing acetylene black concentration (20%). At 300 °C sintering temperature, a maximum specific surface area of ~45 m^2 g^{-1} was obtained. In CC mode at 0.05 C rate, test cells exhibited first discharge capacities of ~123 and ~165 mA h g^{-1} for charge cut-off voltages of 4.4 and 5.0 V, respectively. It could be seen that discharge capacity retentions of 80 and 92% were noted at 0.2 and 0.5 C rates after 100 cycles. On the other hand, using CC–CV mode (charge cut-off 4.4 V), the cell also exhibited an initial discharge capacity of 147, 145, 123, and 65 mA h g^{-1} at 0.05, 0.1, 1 and 10 C rates. Dry ball milling was also reported by the same authors to increase the surface area to a greater extent than wet milling (over 100 m^2 g^{-1}).[103] It is surprising to notice that the cell delivered a discharge capacity of ~75 and 140 mA h g^{-1} at room temperature and 55 °C respectively at 0.05 C (CC mode between 2.5 and 4.4 V). In the elevated temperature operation, the polarization of the electrode was found to be minimum compared to that at room temperature. The high surface area C–$LiMnPO_4$ displayed good rate capability performance, for example the cell displayed discharge capacities of 140, 130, 120, 90, 77, and 60 mA h g^{-1} at 0.05, 0.1, 0.2, 0.5, 1, and 2 C, respectively. Moreover, various kinds of carbon were also used for the milling, for example acetylene black (surface area: 68 m^2 g^{-1}) and two types of ketjen black (KB) with different surface areas (surface area: 800 and 1400 m^2 g^{-1}).[101] The composite C–$LiMnPO_4$ was prepared by wet ball milling followed by calcination at 500 °C for 4 h in the above mentioned atmosphere. The $LiMnPO_4$/high surface area KB composite cathode delivered a discharge capacity of 166 mA

h g^{-1} at 0.05 C in the CC mode, which is about 97% of the theoretical value of $LiMnPO_4$. Spherical shape particles of C–$LiMnPO_4$ were also prepared by the same group using spray pyrolysis and subsequent wet ball milling with acetylene black (20%).[102] Electrochemical cells containing the spherical C–$LiMnPO_4$ microparticles exhibited first discharge capacities of 112 and 130 mA h g^{-1} at 0.05 C at room temperature and 55 °C, respectively. These also showed a good rate capability up to 5 C at room temperature and 55 °C as well.

The solid-solution between $LiMnPO_4$ and $LiCoPO_4$ was also reported by the same group using the spray pyrolysis technique.[105] The prepared $LiCo_xMn_{1-x}PO_4$ ($x = 0$, 0.2, 0.5, 0.8, and 1) powders were milled with 10 wt% acetylene black in ethanol by planetary high-energy ball-milling to form composites with carbon. The cells were tested at a 0.05 C rate and delivered an initial discharge capacity of 165 mA h g^{-1} at $x = 0$, 136 mA h g^{-1} at $x = 0.2$, 132 mA h g^{-1} at $x = 0.5$, 125 mA h g^{-1} at $x = 0.8$ and 132 mA h g^{-1} at $x = 1.0$, respectively. The discharge capacity of the C–$LiCo_xMn_{1-x}PO_4$ nanocomposite cathode gradually decreases with increase of cycle number. The capacity retentions of C–$LiMnPO_4$, C–$LiCo_{0.2}Mn_{0.8}PO_4$, C–$LiCo_{0.5}Mn_{0.5}PO_4$, C–$LiCo_{0.8}Mn_{0.2}PO_4$ and C–$LiCoPO_4$ nanocomposites were 60, 62, 66, 61 and 49%, respectively, over 100 cycles. The discharge capacities of C–$LiCo_{0.2}Mn_{0.8}PO_4$ and C–$LiMnPO_4$ nanocomposites quickly decrease to approximately the 20th cycle and then gradually decrease with cycle number compared with C–$LiCoPO_4$ nanocomposites. Finally, it is interesting to note that cyclability of the C–$LiCo_{0.5}Mn_{0.5}PO_4$ nanocomposite cathode was neutralized by two types of electrochemical behaviors of C–$LiMnPO_4$ and C–$LiCoPO_4$ nanocomposites.

Oh *et al.*[106–108] continued the work of ultrasonic spray pyrolysis initiated by Taniguchi and co-workers[100–105] with spherical size $LiMnPO_4$ particulates. Carbon coating over the particulates was employed by mixing with sucrose which was followed by ball milling at a speed of 100 rpm for 20 h and subsequently heat treating with different calcination temperatures (550, 650 and 700 °C in Ar–H_2 atm.). Ball milling followed by a sintering process led to the destruction of the spherical shape morphology and the final carbon content in the composite was found to be ~3 wt%. It is obvious that increasing the calcination temperature results in increase in crystallite size (52, 56 and 60 nm for 550, 650 and 700 °C) and decease in specific surface area (69, 66 and 60 m^2 g^{-1} for 550, 650 and 700 °C). Electrochemical properties of $LiMnPO_4$ were conducted in CC–CV mode at 0.05 C (assuming that 1 C = 170 mA h g^{-1}) between 2.7 and 4.5 V *vs.* Li. The discharge capacity of the C–$LiMnPO_4$ powder prepared at 650 °C was 118 mA h g^{-1}, whereas that of C–$LiMnPO_4$ powder calcined at 550 and 700 °C was 90 and 44 mA h g^{-1}, respectively. After 15 cycles, the capacity retention of the C–$LiMnPO_4$ electrode prepared at 650, 550 and 700 °C was about 97.3, 92.5 and 78.5% of its initial discharge capacity, respectively. Further, the authors continued the work on different carbon source materials, such as sucrose with acetylene black (AB) using the same synthesis procedure by tuning other parameters like calcination temperature, time and atmosphere to obtain the best performing material.[108] In this case, the pyrolysed powders were mixed with different ratios (10, 20, 30 and 40 wt%) of AB during ball milling and subsequently heat treated at 500 °C for 1 h under Ar flow. Further, 7.5 wt% carbon black was also included during the fabrication of the electrode. The composite C–$LiMnPO_4$ comprising 30 wt% carbon exhibited a maximum discharge capacity of 158 mA h g^{-1} at 0.05 C by CC–CV mode (it was fixed until the current dropped to 0.01 C). The above-mentioned composite retains 88% of its initial discharge capacity at 55 °C, which is similar to that of room temperature performance. However, the capacity fading was noted for all the composites in elevated temperature operations rather than room temperature conditions. This is possibly due to Mn dissolution in electrolyte solutions (1 M $LiPF_6$ in EC : DEC 1 : 1 vol) and it was found that less dissolution occurred when a 30 wt% carbon comprising composite (319.6, 202.7, 103.7 and 259.9 ppm for 10, 20, 30 and 40 wt% of AB, respectively) was used.

Recently, the same group reported $LiMn_{1-x}Fe_xPO_4$ ($x = 0$, 0.5 and 0.15) powders by an ultrasonic spray pyrolysis followed by ball milling with AB carbon (30 wt%) 106. However, there was no appreciable variation in the electronic conductivity noted for Fe substitution. The Li/C–$LiMnPO_4$ cell exhibited a reversible plateau around 4.1 V *vs.* Li corresponding to the redox couple of Mn^{3+}/Mn^{2+} whereas the C–$LiMn_{0.85}Fe_{0.15}PO_4$ electrode showed two plateaus at 4.1 and 3.5 V *vs.* Li related to Mn^{3+}/Mn^{2+} and Fe^{2+}/Fe^{3+} couples, when cycled between 2.7 and 4.5 V (CC–CV mode) at 0.05 C. The C–$LiMn_{0.85}Fe_{0.15}PO_4$ electrode delivered a slightly higher discharge capacity of 163 mA h g^{-1} than the C–$LiMnPO_4$ electrode (158 mA h g^{-1}). With regard to performances of the cells at elevated temperature (55 °C), reversible capacities of 151 and 137 mA h g^{-1} for bare and Fe doped $LiMnPO_4$ were noted at 0.5 C rate in the above potential window. However, the capacity retention of C–$LiMnPO_4$ at 55 °C dropped to 87%, whereas C–$LiMn_{0.85}Fe_{0.15}PO_4$ exhibited enhanced capacity retention of 91%. Mn dissolution in the electrolyte was found to be 87 ppm for C–$LiMn_{0.85}Fe_{0.15}PO_4$, which was slightly lower than that of the bare compound (104 ppm).

1.5 Precipitation route

A low temperature, 'chimie douce' method was employed for the preparation of native $LiMnPO_4$ in aqueous medium by Delacourt *et al.*[109–111] The prepared materials were ball milled with carbon to prevent agglomeration of the particle as well as to enable carbon coating. The final C–$LiMnPO_4$ composite comprised 16.7 wt% of carbon and the material was directly deposited into an Al current collector without any binder. The ball milled C–$LiMnPO_4$ was tested in Swagelok configuration and exhibited a stable discharge capacity of ~70 mA h g^{-1} for about 15 cycles when cycled between 2 and 5 V at 0.05 C rate by CC mode. Later, the same authors reported stable cycling performances of ~90 mA h g^{-1} at room temperature between 2 and 5 V with the materials prepared by the same approach and having a similar carbon content.[111] As expected, at 50 °C the test cells rendered good cycling performance compared to room temperature cycling with a distinct plateau around 4.1 V *vs.* Li. The authors revealed that the poor performance at room temperature was mainly because of the wide band gap between

conduction and valance bands (~1.14 eV) when compared to $LiFePO_4$ (between 0.39 and 0.5 eV), which results in the insulating behavior of the material. The electronic conductivity of C–$LiMnPO_4$ was measured by ac impedance spectroscopy and was found to be $\sim 2.7 \times 10^{-9}$ S cm^{-1} at 300 °C. A similar kind of co-precipitation technique ($MnPO_4 \cdot H_2O$) was also reported by Xiao *et al.*[112] by varying the calcination temperature from 350 to 550 °C. The above precursors were ball milled with lithium acetate and 20 wt% carbon to obtain C–$LiMnPO_4$. C–$LiMnPO_4$ prepared at 500 °C exhibited a discharge capacity of ~115 mA h g^{-1} at 0.05 C between 2.5 and 4.4 V in CC–CV mode. The cell showed 73% capacity retention after 60 cycles. C–$LiMnPO_4$ prepared at 350 °C showed a discharge capacity of ~60 mA h g^{-1} under the same test conditions with huge polarization (~400 mV) and a shortened two phase region though particle sizes were quite smaller. This clearly indicates that the crystallization of the phase was more important rather than the particle size. Non-stoichiometric proportions of lithium deficient ($Li_{0.5}MnPO_4$ and $Li_{0.8}MnPO_4$) and rich phases ($Li_{1.1}MnPO_4$ and $Li_{1.2}MnPO_4$) were also synthesized and reported by Xiao *et al.*[113] using the same co-precipitation followed by a solid-state approach with ball-milling of carbon. In all the non-stoichiometric compounds of Li_xMnPO_4 phases, traces of impurities like $Mn_2P_2O_7$ or Li_3PO_4 unavoidably co-existed with the native phase. The observed impurity phases were consistent with the phases observed in other olivine compounds such as $LiFePO_4$.[114,115] The half-cells comprising $LiMnPO_4$, $Li_{1.1}MnPO_4$ and $Li_{1.2}MnPO_4$ phases displayed almost the same initial discharge capacity of ~124 mA h g^{-1} at 0.05 C rate between 2 and 4.5 V by CC–CV mode, whereas $Li_{0.5}MnPO_4$ and $Li_{0.8}MnPO_4$ exhibited ~75 and 110 mA h g^{-1}, respectively. $Li_{1.1}MnPO_4$ showed extremely stable performance of ~130 mA h g^{-1} in the 80th cycle. The $LiMnPO_4$ and $Li_{1.2}MnPO_4$ phases were experiencing a meager amount of capacity fade and showed a discharge capacity of ~115 in the 40th cycle. The authors claimed that the improved performance of the $Li_{1.1}MnPO_4$ phase was due to the presence of an appropriate amount of highly ionically conducting Li_3PO_4, which improves the Li-ion transport properties. On the other hand, the presence of a huge amount of Li_3PO_3 will impede the transportation of electrons and this was noted in the case of the $Li_{1.2}MnPO_4$ phase. In Li-deficient phases, a trend of increasing capacity was noted for both $Li_{0.5}MnPO_4$ and $Li_{0.8}MnPO_4$, and discharge capacities of ~110 and ~150 mA h g^{-1}, respectively, were delivered in the 90th cycle.

Ma and Qin[116] reported the synthesis of nanocrystalline $LiMPO_4$ (M = Fe and Mn) by electrostatic spray deposition (ESD) combined with the sol–gel technique for the first time. The prepared materials were subjected to heat treatment in an Ar atmosphere at 600 °C to attain a uniform nanocrystalline phase (~50 nm). However, the prepared Li/$LiMnPO_4$ cells delivered only about ~20 mA h g^{-1} as discharge capacity, when the cell was cycled between 3 and 4.5 V at 5 μA cm^{-2}. The cyclic voltammogram revealed the asymmetric behavior of the fabricated cell and the peak separation between the anodic and cathodic scan was about ~300 mV because of the presence of the strong polarization of $LiMnPO_4$.

Oh *et al.*[117] reported the reduction of polarization of the electrode and the least amount of Mn dissolution in C–$LiMn_{0.5}Fe_{0.5}PO_4$ by a precipitation technique. Initially, olivine $LiMn_{0.5}Fe_{0.5}PO_4$ was carbon coated with carbon (3.3 wt%) and it delivered a discharge capacity of ~125 and ~140 mA h g^{-1} at 0.05 C rate at room temperature and 55 °C, respectively, between 2.7 and 4.5 V *vs.* Li by CC–CV mode. The same group reported the performance of micron-sized nanoporous C–$LiMn_{0.85}Fe_{0.15}PO_4$ with high volumetric capacity.[118] The capacity delivered by the micron-$LiMn_{0.85}Fe_{0.15}PO_4$ electrode was nearly 1.4 times higher than that of the nano-$LiMn_{0.85}Fe_{0.15}PO_4$ electrode, *i.e.*, 369.3 mA h cm^{-3} *versus* 261.1 mA h cm^{-3} under the above test conditions. However, the reverse trend was noted for gravimetric capacities of ~160 and ~140 mA h g^{-1} for nano and micron-sized C–$LiMn_{0.85}Fe_{0.15}PO_4$ powders, respectively. Double structured $LiMn_{0.85}Fe_{0.15}PO_4$ coordinated with $LiFePO_4$ was also reported by Oh *et al.*[119] The core contained $LiMn_{0.85}Fe_{0.15}PO_4$ to enable high energy density and the outer layer was composed of $LiFePO_4$ to facilitate high rate capability. Carbon was also coated over the outer layer to increase the electronic conductivity.

1.6 Hydro/solvo/iono-thermal routes

Fang *et al.*[120,121] reported the successful preparation of $LiMnPO_4$ plates by a simple hydrothermal route in basic medium at 200 °C. The results clearly indicate that the prepared materials were in the real nanometric range and actively participated in the electrochemical reaction in which plate-like $LiMnPO_4$ ball milled with 20% of carbon delivered a discharge capacity of 68 mA h g^{-1} between 3 and 4.5 V at 1.5 mA g^{-1} and the cell presented a prominent plateau around 4.1 V *vs.* Li.

Divalent cation doping (10%), such as Mg, Ni, Co, Zn and Cu, was reported by Chen *et al.*[122] *via* a hydrothermal approach. The substitution on Mn sites leads to a decrease in lattice parameter values. The cell volume also decreased 0.8% for Mg^{2+}, 0.6% for Ni^{2+}, 0.3% for Cu^{2+}, and 0.4% for Zn^{2+} substitution consistent with their smaller ionic radii. The presence of the larger divalent cations was more compatible with the olivine structures, and stabilized the lattice against strain created by the small Jahn–Teller Mn^{3+} ions. Further, it is well known that the delithiated $LiMnPO_4$ ($Li_{0.1}MnPO_4$) phase was highly reactive in air. However, the divalent substitution (for example, Mg^{2+}) on Mn sites resulted in decreased reactivity of $Li_{0.1}Mg_{0.1}Mn_{0.9}PO_4$ in air as well as prevented the formation of larger crystalline domains in Mg-substituted materials. This in turn creates a more favorable boundary between the two phases and facilitates the conversion of one phase to the other without loss of coherence.

A citric acid assisted facile one step solvothermal (equiv. volume mixture of water and ethanol) procedure was adopted by Wang *et al.* to synthesize the microspherical $LiMnPO_4$ at 300 °C.[123,124] The obtained microspherical particles were mixed with glucose followed by heat treatment for carbon coating. The Li/$LiMnPO_4$ cell displayed a discharge capacity of 107 mA h g^{-1} at 0.01 C with an appreciable plateau around ~4.1 V *vs.* Li. As expected, increasing the current rate leads to poor cell performance; for example, at 1 C the test cell presented a discharge

capacity of 49 mA h g^{-1}. By introducing cetyltrimethylammonium bromide (CTAB) as a chelating agent in the above solvent mixture at relatively low temperature conditions (240 °C), $LiMnPO_4$ nanorods can be obtained.[124] The obtained $LiMnPO_4$ nanorods were mixed with dextrose for carbon coating and fired at 700 °C for 5 h under Ar to yield C–$LiMnPO_4$. The prepared composite material exhibited an initial discharge capacity of ~127 mA h g^{-1} at a constant current of 0.01 C. The diffusion co-efficient in the C–$LiMnPO_4$ phase was calculated as 5.056×10^{-14} cm^2 s^{-1}.

The storage performance of nanoplatelets of $LiMnPO_4$ and $LiFe_{0.5}Mn_{0.5}PO_4$ was studied by Saravanan *et al.* using a simple solvothermal method at 250 °C for 8 h with gluconic acid D-lactone.[125] The final $LiMnPO_4$ and Fe doped phases comprised of 10 wt% carbon. The test cells exhibited a discharge capacity of ~50 and 65 mA h g^{-1} for native and Fe doped phases, respectively at 17 mA g^{-1} between 2.3 and 4.5 V by CC mode. Further, the same group of authors continued the work on solid-solutions of $LiMn_{1-x}Fe_xPO_4$ (where, $x = 0.25$, 0.5 and 1) nanoplates by tuning various parameters, such as source materials, precursor concentration, effect of solvent, synthesis temperature and conducting coatings using the same approach.[126] The obtained olivine phase powders were ball milled with carbon before making the slurry. The synthesized native phase $LiMnPO_4$ was decorated with silver, gold and carbon (derived from gluconic acid D-lactone) to alleviate the intrinsic behaviour. However, in CC mode the performance of the material was poor due to the heterogeneous coating of Ag and Au. Then, the authors prepared the solid-solutions of C–$LiFe_{0.5}Mn_{0.5}PO_4$ and C–$LiFe_{0.25}Mn_{0.75}PO_4$ and those materials delivered discharge capacities of 127 mA h g^{-1} (at 0.02 C) and ~35 mA h g^{-1} (at 0.01 C), respectively, cycled between 2.3 and 4.5 V by CC mode. The increase in capacity was noted in the C–$LiFe_{0.5}Mn_{0.5}PO_4$ plates; for example in the 10th cycle the cell showed a discharge capacity of ~153 mA h g^{-1}. The cell (Li/C–$LiFe_{0.5}Mn_{0.5}PO_4$) exhibited good capacity retention at high current rates, 120, 104, 91, 79, and 60 mA h g^{-1} for 1, 3, 5, 7 and 10 C rates, respectively. Long term cycling up to 1000 cycles was evaluated for the Li/C–$LiFe_{0.5}Mn_{0.5}PO_4$ cell at 2 C rate with columbic efficiency over 98%. However, the obtained results were slightly contrary to the theoretical predictions of the $LiFe_{0.5}Mn_{0.5}PO_4$ system by Gardiner and Islam[127] and they concluded the following three points. (i) The most favourable intrinsic defect was the anti-site defect (a small population (<2%) of Li^+ and Fe^{2+} or Mn^{2+} ions was expected to exchange sites). (ii) Significant binding energies (>−0.6 eV) were found for neutral one-dimensional clusters along the *b*-axis channel comprised of anti-site defects and Li vacancies. This has implications for lithium conductivity as Fe or Mn cations on Li sites could lead to trapping of the migrating Li^+ vacancies. Defect clustering therefore may inhibit Li extraction, in which defect cluster regions were more likely to retain lithium. (iii) The higher anti-site migration energy in $LiFe_{0.5}Mn_{0.5}PO_4$ compared to pure $LiFePO_4$ suggests that any anti-site defects in this mixed-metal system would have a greater blocking effect on lithium insertion/extraction rates. Flowerlike morphologies of $LiMnPO_4$ were also reported in the solvothermal approach (water and diethyleneglycol mixture as the solvent) which delivered a reversible capacity of ~50 mA h g^{-1}.[128]

Manthiram and co-workers[129–131] reported a facile route to produce nanostructured $LiMnPO_4$ by a microwave assisted hydrothermal or solvo-thermal approach. In the hydrothermal approach glucose was used as the source material for carbon, whereas MWCNTs were painted on the surface to enable a conducting network for $LiMnPO_4$ nanorods by the solvothermal route. $LiMnPO_4$ prepared by the above-mentioned routes displayed a monotonous charge–discharge curve and exhibited a discharge capacity of ~15 to 45 mA h g^{-1}. Ji *et al.*[132] also followed a similar approach to yield $LiMnPO_4$ nanostructures using citric acid and sodium dodecyl benzene sulfonate (SDBS) as an additive to tune the morphology of the final product. Further, the prepared materials were ball milled with 30% acetylene black to form a C–$LiMnPO_4$ composite. The composite was cycled between 2.7 and 4.8 V at 0.05 C by CC mode and it delivered a discharge capacity of 89 and 64 mA h g^{-1} for citric acid and SDBS assisted routes respectively. However, similar to the previous work, the composite $LiMnPO_4$ did not show any obvious plateau around 4.1 V *vs.* Li.

Chen *et al.*[133] reported the kinetic behavior during Mg^{2+} substitution on Mn sites and the compounds were prepared by a hydrothermal reaction and consequently ball milled with carbon (20 wt%) before making electrodes. Increasing the concentration of Mg^{2+} ($LiMn_{1-x}Mg_xPO_4$, $x = 0 \leq 5$) provides substantial improvement in the thermal stability of the phase. Further, Mg^{2+} dilutes the concentration of the Jahn–Teller active ion Mn^{3+} and reduces local strains between the phases, thereby increasing the structural stability of the phase. As expected, the substitution of Mg^{2+} results in decrease in unit cell volume while increasing the concentration and improvement in kinetic property as well.

Various shapes, such as nano-squares, bows, spindles and cubes, of $LiMnPO_4$ were prepared and reported using $Na_4P_2O_7 \cdot 10H_2O$ by Li *et al.*[134] The obtained phases were modified using ascorbic acid and fired at 600 °C to achieve carbon coating. Among the various shapes, nanosquares showed the maximum reversible capacity of 82 mA h g^{-1} when compared to spindles (49 mA h g^{-1}), bows (29 mA h g^{-1}) and cubes (61 mA h g^{-1}) while cycling between 2.5 and 4.9 V at 0.1 C by CC mode. Carbon coating was also carried out for nanosquares using ascorbic acid and the cell displayed an initial discharge capacity of 126 mA h g^{-1} at 0.1 C. After 50 cycles, C–$LiMnPO_4$ displayed a discharge capacity of 87 mA h g^{-1}, whereas only 66% of the initial discharge capacity was retained for bare $LiMnPO_4$ nanosquares.

Ni and Gao[135] reported the synthesis of Cu^{2+} substituted $LiMnPO_4$ by an ascorbic acid mediated synthesis. The obtained particles (~100 nm) were carbon coated by carbonization of sucrose at 600 °C and a carbon content of 2.4 wt% was obtained in the final product. In the range of 2.2–4.5 V (CC–CV mode), test cells delivered a reversible capacity of 101, 121 and 76 mA h g^{-1} for $LiMnPO_4$, $LiMn_{0.98}Cu_{0.02}PO_4$ and $LiMn_{0.95}Cu_{0.05}PO_4$ phases, respectively. Cu^{2+} doping can bring about new impurity energy levels in the forbidden band, and thus increase the electronic conductivity. Nevertheless, it will block the one dimensional diffusion channel for Li-ion transportation, which leads to the

degradation of ionic conductivity. In the case of Cu^{2+} doping, only 0.2% of Li sites were occupied by the dopant for $LiMn_{0.98}Cu_{0.02}PO_4$, whereas 1.8% of Li sites were occupied by $LiMn_{0.95}Cu_{0.05}PO_4$. The latter compound significantly impedes the transportation of Li ions, which leads to the poor performance of the cell. Further, the same group reported the synthesis of $LiMnPO_4$ by a solid state reaction along with a certain amount of sucrose (expected to produce 2 wt% of carbon) followed by high energy ball milling with (8 wt%) or without carbon using a high speed planetary miller.[136] A discharge capacity of 83, 135 and 127 mA h g^{-1} was obtained for pristine $LiMnPO_4$, $LiMnPO_4$ ball milled with carbon and $LiMnPO_4$ ball milled without carbon, respectively, when cycled between 2.2 and 4.5 V (CC–CV mode) at 0.05 C rate at room temperature. At 55 °C the material milled with carbon rendered a stable capacity of ~135 mA h g^{-1} for about 40 cycles in the CC–CV protocol.

Wang *et al.*[137] reported the solvothermal synthesis of $LiMnPO_4$ nanoplates and rods using sodium dodecyl benzene sulfonate (SDBS). The synthesized powders were carbon coated through chemical vapor deposition (CVD) using methylbenzene as the carbon source and argon as the carrier gas. The authors compared the carbon coating technique with the conventional high energy ball milling (BM) procedure. The discharge capacities of Plate-CVD, Rod-CVD, Plate-BM and Rod-BM were 147, 126, 120 and 92 mA h g^{-1}, respectively, between 2.5 and 4.9 V at 0.05 C at room temperature by CC mode. Capacity retention of 93, 90, 85 and 81% was observed after 50 cycles for Plate-CVD, Rod-CVD, Plate-BM and Rod-BM, respectively. The improved performance of Plate-CVD was mainly due to the shorter diffusion pathways for the *b* direction and $LiMnPO_4$ platelets were highly encapsulated with carbon using CVD.

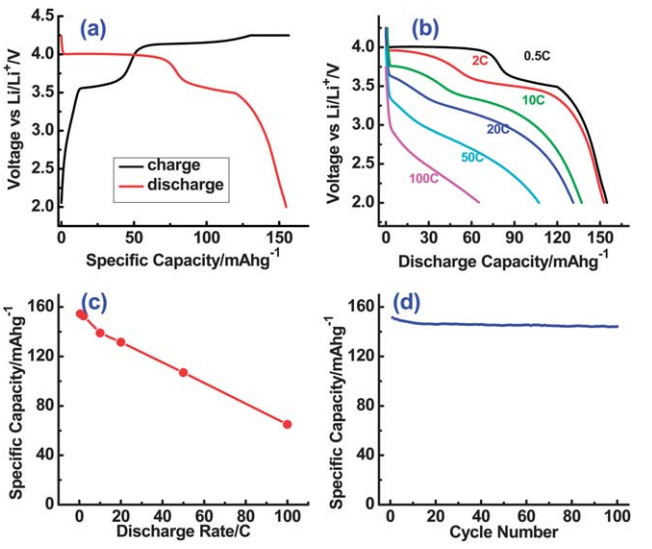

Fig. 7 Electrochemical characterizations of the $LiMn_{0.75}Fe_{0.25}PO_4$ nanorod cathode grown on rmGO. (a) Representative charge and discharge curves of $LiMn_{0.75}Fe_{0.25}PO_4$ nanorods grown on rmGO at a rate of 0.5 C. (b) Discharge curves of $LiMn_{0.75}Fe_{0.25}PO_4$ nanorods on rmGO at various C rates. (c) Specific discharge capacities of $LiMn_{0.75}Fe_{0.25}PO_4$ nanorods on rmGO at various C rates. The discharge cut-off voltage was 2.0 V *vs.* Li. (d) Capacity retention of $LiMn_{0.75}Fe_{0.25}PO_4$ nanorods on rmGO at a rate of 0.5 C.[139] Copyright: John Wiley & Sons, Inc.

Recently, Dokko *et al.*[138] suggested the synthesis of $LiMnPO_4$ nanoparticles by reacting Li_3PO_4 (solid) with molten aqua-complexes of $MnSO_4$ under hydrothermal conditions at 190 °C. Later, the obtained $LiMnPO_4$ particles were carbon coated using sucrose with subsequent heat treatment at 700 °C. The molar ratio of Mn(II) and H_2O in the reactor was varied by adding water to the reaction mixture. The molar ratio of H_2O and Mn(II) in the reactor is henceforth abbreviated as x = [mole of H_2O]/[mole of $MnSO_4$]. When, x = 7.8, 50 nm size $LiMnPO_4$ particles were obtained which delivered a discharge capacity of ~135 mA h g^{-1} at 0.1 C between 2 and 4.5 V by CC–CV mode. The cell also displayed good rate performance at 1 C and showed ~83 mA h g^{-1} as discharge capacity at room temperature. However, no cyclability has been reported.

Wang *et al.*[139] reported a two step synthesis of a graphene grown $LiMn_{0.75}Fe_{0.25}PO_4$ nanorod hybrid system. In the first step, Fe-doped Mn_3O_4 nanoparticles $(Mn_{0.75}Fe_{0.25})_3O_4$ were first selectively grown onto mildly oxidized graphene oxide (mGO) by controlled hydrolysis. Later, LiOH and H_3PO_4 were used to obtain the desired olivine phase material by the solvothermal approach, in which ascorbic acid ($C_6H_8O_6$) was used to reduce Fe^{3+} to Fe^{2+} and mGO as well. The electrical conductivity showed dramatic enhancement in the $LiMn_{0.75}Fe_{0.25}PO_4$/reduced mildly oxidized graphene oxide (rmGO) hybrid system (0.1–1 S cm^{-1}) which is 10^{13} to 10^{14} times higher than pure $LiMnPO_4$. Nanorods with the size of 50–100 nm length and 20–30 nm width were grown in the preferential (0 0 1) direction. $LiMn_{0.75}Fe_{0.25}PO_4$-rmGO delivered an initial discharge capacity of 155 mA h g^{-1} and showed stable capacity behavior upto 100 cycles at 0.5 C between 2 and 4.25 V by CC–CV mode at room temperature. The $LiMn_{0.75}Fe_{0.25}PO_4$–rmGO hybrid system rendered excellent rate performance, for example 153, 132, 107 and 65 mA h g^{-1} for 2, 20, 50 and 100 C rates, respectively. The cycling performance of the $LiMn_{0.75}Fe_{0.25}PO_4$–rmGO hybrid system is given in Fig. 7. So far, this is one of the best values obtained for an $LiMnPO_4$ based system and the values are comparable to the well known commercially available materials ($LiCoO_2$, $LiMn_2O_4$ and $LiFePO_4$) and their solid-solutions reported by other authors, whereas a simple mixture of $LiMn_{0.75}Fe_{0.25}PO_4$ and rmGO showed poor performance capable of delivering 75 and 44 mA h g^{-1} at 0.1 and 1 C rates, respectively, under the same test conditions.

Tarascon and co-workers[140] introduced the synthesis of $LiMnPO_4$ by ionothermal reactions using various kinds of ionic liquids and in such a way the morphology was also tuned. Carbon coating was achieved by high energy ball milling (15 min) with sucrose (20 wt%) and subsequent heat treatment at 700 °C in a quartz tube for about 5 min. The carbon coated $LiMnPO_4$ showed a reversible capacity of ~95 mA h g^{-1} at 0.05 C between 2.5 and 4.6 V by CC mode, whereas uncoated $LiMnPO_4$ delivers a capacity of ~35 mA h g^{-1}. Binary mixtures of ionic liquids and diols (1,2-propanediol or 1,3-propanediol) were also used to synthesize the above compound which was subsequently carbon coated using sucrose. Diol assisted carbon-coated $LiMnPO_4$ exhibited a maximum capacity of ~82 mA h g^{-1} for 1,2-propanediol at room temperature.

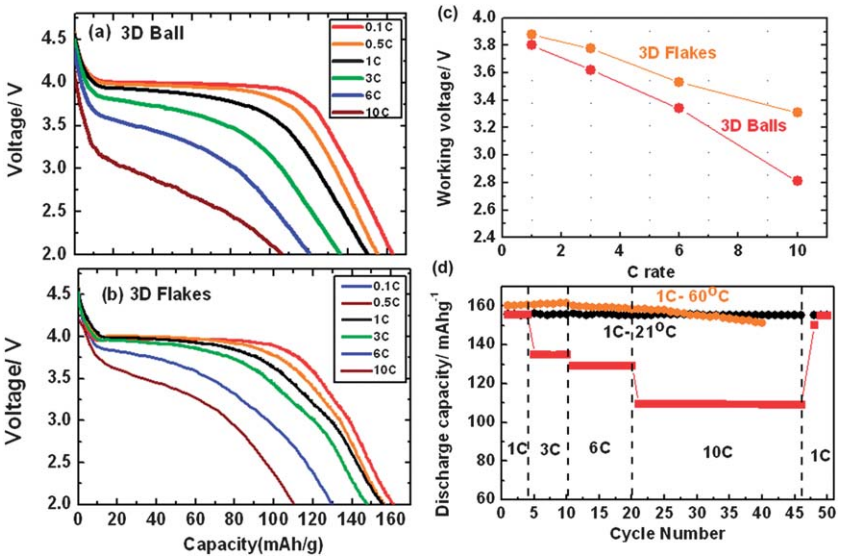

Fig. 8 (a and b) Voltage profiles of 3DM LMP balls and flakes in coin-type half cells at 21 °C and the cells were charged to 4.6 V (*vs.* Li/Li$^+$) at a 0.1 C rate and kept at 4.6 V for 2 h, and discharged to 2 V at different C rates (0.1, 0.5, 1, 3, 6, and 10 C) (the cells were tested at 21 °C and 1 C was set at 170 mA g^{-1}). (c) Plot of working voltages (voltage in half of the discharge capacity value) as a function of C rate from the above curves. (d) Discharge capacity *vs.* cycle number of 3DM-flakes at 1 C under 21 °C and 60 °C cyclings in coin-type half cells and discharge capacity *vs.* cycle number at different C rates from 1 to 10 C at 21 °C. For a 60 °C test, the cell was discharged to 2 V at a 1 C rate and was charged to 4.6 V at a 1 C rate, and held at that voltage for 3 h.[141] Copyright: John Wiley & Sons, Inc.

1.7 Template mediated approach

Yoo *et al.*[141] reported the synthesis of 3D macroporous-$LiMnPO_4$ showing ball and flake-like morphology, which was synthesized using a polymethylmethacrylate (PMMA) template approach. For the preparation of such unique morphology, a 500 mm thick n-type silicon substrate with a ⟨100⟩ orientation was used. The template was first annealed at 300 °C under an Ar flow for 2 h and increased to 500 °C for 1 or 2 h to obtain crystallized and carbon coated $LiMnPO_4$. The final product was scratched from the Si substrate after annealing. High specific surface areas of 21 and 29 m^2 g^{-1} were noted for 3DM balls and flakes, respectively. The 3DM balls delivered a discharge capacity of 162 mA h g^{-1} (at 0.1 C rate) between 2 and 4.6 V by CC–CV mode at 21 °C. Capacities of 154, 150, 135, 120 and 105 mA h g^{-1} were noted for the rates of 0.5, 1, 3, 6, and 10 C, respectively. Though 3DM-flakes delivered a discharge capacity similar to that of 3DM balls at 0.1 C, at high current rates, an improvement in the discharge capacity was noted, *i.e.* 155, 154, 147, 129, and 110 mA h g^{-1} for 0.5, 1, 3, 6, and 10 C rates, respectively. At 60 °C, the 3DM-flakes experienced only 2% of capacity fade up to 40 cycles tested with a capacity of ~160 mA h g^{-1}. The electrochemical performance of the 3DM-flakes and balls is illustrated in Fig. 8.

1.8 Supercritical ethanol process

Honma and co-workers[142,143] reported the synthesis and electrochemical performance of $LiMnPO_4$ nanocrystals by a supercritical fluid process in ethanol medium. The crystal sizes were effectively adjusted by varying the concentration of oleylamine. Then the crystals were ball-milled to yield C–$LiMnPO_4$ with acetylene black and vapour grown carbon nanofibers with subsequent heat treatment at 600 °C under an Ar–H_2 atmosphere. The Li/C–$LiMnPO_4$ cell showed discharge capacities of 153 and 62 mA h g^{-1} at 0.01 and 0.5 C between 2 and 4.5 V by CC mode at room temperature. The effect of particle size was also investigated and discharge capacities of ~90, ~120 and ~160 mA h g^{-1} at 0.01 C were achieved for 100, 60 and 20 nm sizes of the crystals respectively.

2 Experimental section

Scalable solid state reactions were employed for the synthesis of $LiMnPO_4$ particles. In a typical synthesis procedure, stoichiometric amounts of Li_2CO_3, MnO and $NH_4H_2PO_4$ were mixed thoroughly and decomposed at 400 °C for 4 h to decompose the ammonium moieties. Then, the resultant materials were again ground and made as a pellet and fired at 850 °C for 6 h in an Ar atmosphere to yield resultant single phase $LiMnPO_4$ particles. Carbon coating was performed by milling with 25 wt% super P carbon $LiMnPO_4$ for 8 h using a SPEX 8000D, USA. Powder X-ray diffraction patterns were recorded using a Bruker AXS, D8

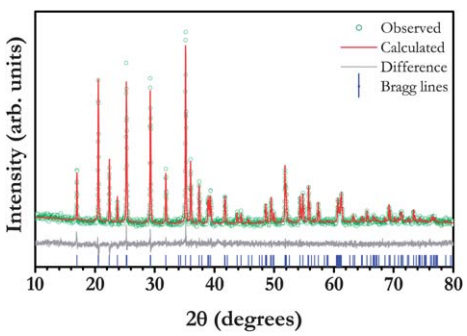

Fig. 9 Powder X-ray diffraction pattern of carbon coated $LiMnPO_4$ synthesized at 850 °C under an Ar atmosphere.

Advance with Cu Kα radiation. The Rietveld refinement was conducted using Topas V3 software. Morphological features were analyzed using a field emission scanning electron microscope (FE-SEM, JEOL JSM-7600F) and transmission electron microscope (TEM, JEOL 2100F). Electrochemical characterization was carried out using the two electrode CR 2016 coin-cell configuration. The composite cathodes were prepared by pressing accurately weighed 20 mg of the prepared material (C–$LiMnPO_4$) and 3 mg of Teflonized acetylene black (TAB) mixture on a 200 mm^2 stainless steel mesh and subsequently dried at 60 °C in a vacuum oven for 6 h. The test cell was fabricated in an argon filled glove box by pressing the composite cathode and lithium metal anode separated by a microporous glass fiber separator (Whatman, Cat. no. 1825 047, UK). 1 M $LiPF_6$ in an ethylene carbonate (EC)–diethyl carbonate (DEC) (1 : 1 wt%, DAN VEC) mixture was used as the electrolyte solution. Galvanostatic cycling performances were carried out using an Arbin 2000 battery tester.

3 Discussion

Fig. 9 presents the powder X-ray diffraction pattern of $LiMnPO_4$ synthesized at 850 °C in an Ar atmosphere. The observed reflections clearly indicate the formation of single phase $LiMnPO_4$ without any traces of starting materials or impurity phases like MnO and Li_3PO_4. The structure of $LiMnPO_4$ is analogous to the $LiFePO_4$ system comprising a hexagonal closed-packing (hcp) of oxygen atoms with Li^+ and Mn^{2+} cations located in half of the octahedral sites and P^{5+} cations in 1/8 of the tetrahedral sites.[144] This structure may be described as chains (along the *c* direction) of edge-sharing MnO_6 octahedra which are cross-linked by the PO_4 groups forming a three-dimensional (3-D) network. Tunnels perpendicular to the [010] and [001] directions contain octahedrally co-ordinated Li^+ cations (along the *b* axis), which are mobile in these cavities. The distorted arrangement of MnO_6 octahedra provides poor conductivity profiles. These compounds generally crystallize in the orthorhombic structure with the *Pnmb* space group. The obtained reflections were refined using Rietveld refinement and lattice parameters were also calculated: $a = 6.1018(9)$ Å, $b = 10.4439(5)$ Å and $c = 4.7450(6)$ Å. The obtained values are consistent with the literature (JCPDS #74-0375). The crystallite size was also calculated from the Scherrer equation programmed in Topas software and was found to be 80 nm.

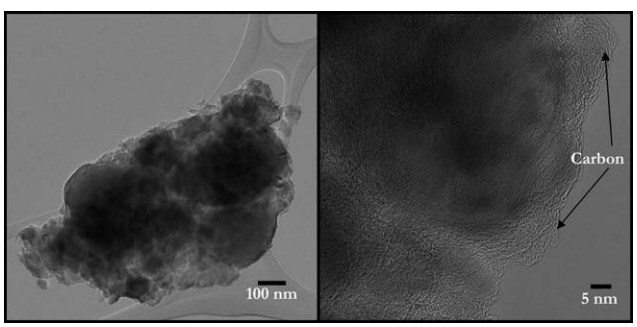

Fig. 10 (a) Transmission electron microscopic picture and (b) HR-TEM image of C–$LiMnPO_4$.

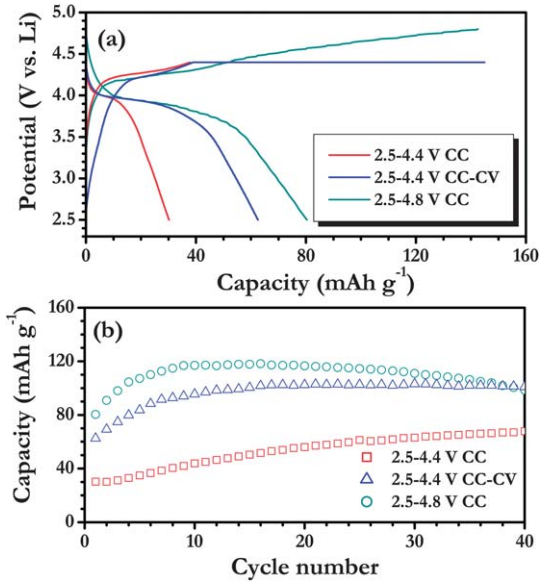

Fig. 11 (a) Initial charge–discharge curves and (b) cycling profiles of Li/C–$LiMnPO_4$ half-cells tested with three different conditions at room temperature (25 °C).

Morphological features of the prepared carbon coated-$LiMnPO_4$ particles were recorded using transmission electron microscopy (TEM) and are presented in Fig. 10a. The TEM picture clearly reveals the aggregation of particles and this sort of aggregation was reasonable, since the synthesized $LiMnPO_4$ powders were ball milled with 25% of carbon for about 8 h to enable carbon coating. Obviously, during such high energy ball milling, the micron-sized particles were reduced to a sub-micron size with a pronounced carbon layer on the surface. But still some sub-micron particles with the size of ~200 nm were also seen along with some fine particles embedded in the carbon matrix. The carbon coating is clearly seen from the high resolution-TEM picture with a more or less homogeneous layer on the surface (Fig. 10b). It is well known that the presence of a carbon layer over the $LiMnPO_4$ particulates is beneficial for faster electronic transport, thereby enabling good electronic conductivity of the electrode.

The electrochemical performance of C–$LiMnPO_4$ was evaluated in a half-cell configuration at 0.05 C with three different potential limits in room temperature and it is illustrated in Fig. 11. Fig. 11a corresponds to the initial charge–discharge curves of the Li/C–$LiMnPO_4$ cell. The test cell cycled between 2.5 and 4.4 V delivers a discharge capacity of 30 and ~65 mA h g^{-1} for CC and CC–CV modes respectively with a noticeable plateau around ~4 V irrespective of testing protocols. In CC–CV mode, a constant potential of 4.4 V was fixed for 24 h (until the current drops to 0.005 C rate) to extract Li-ions, whereas the cell cycled between 2.5 and 4.8 V by CC mode delivered a discharge capacity of 80 mA h g^{-1} with huge irreversible capacity. The irreversible capacity was expected, while charging up to 4.8 V involves the decomposition of the electrolyte solution which is

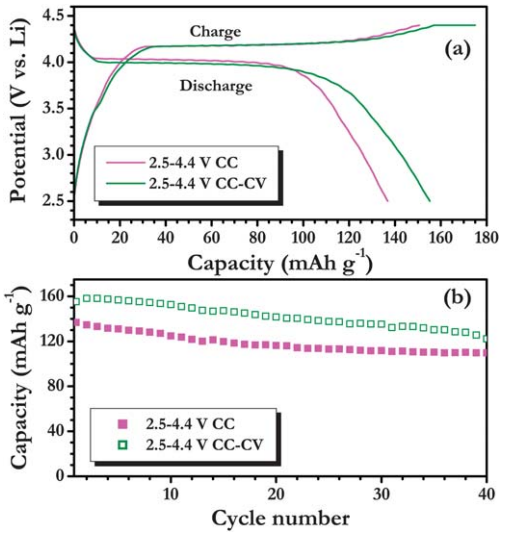

Fig. 12 (a) First charge–discharge curves and (b) cycling profiles of Li/C–$LiMnPO_4$ half-cells tested with two different conditions at elevated temperature (55 °C).

normally stable at ~4.6 V *vs.* Li. All test conditions clearly demonstrated that the extraction of lithium-ion is feasible, irrespective of the synthesis route adopted to prepare the pure phase material with appropriate carbon coating. The cycling profiles under the above three test conditions are given in Fig. 11b. The capacity tends to increase in the initial cycles and such an increase is mainly due to the slower participation in the electrochemical reaction. After 10 cycles, those cells presented discharge capacities of ~45, 100 and 120 mA h g^{-1} for the upper cut-off potential of 4.4 V (CC), 4.4 V (CC–CV) and 4.8 V, respectively. The cells tested at a cut-off potential of 4.4 V delivered quite stable performance up to 40 cycles. However, capacity fading was noted while charging the cell up to 4.8 V, which was mainly because of electrolytic instability. In the case of CC mode, discharge capacity increases with the cycle number and it is stabilized at ~75 mA h g^{-1}. An obvious difference has been noticed between the electrochemical performances of CC and CC–CV modes at room temperature. In the latter mode ~0.15 moles of lithium only can be extracted compared to the former. This difference clearly indicates the poor kinetic behavior of $LiMnPO_4$ particles and it is consistent with Muraliganth and Manthiram's[85] report on GITT measurements.

Elevated temperature (55 °C) performance of C–$LiMnPO_4$ was also evaluated between 2.5 and 4.4 V (CC and CC–CV mode) at 0.05 C and is given in Fig. 12. It is obvious from the initial charge–discharge curves (Fig. 12a), which clearly show a long distinct plateau at ~4 V and ~4.2 V during discharge and charge, respectively, and it corresponds to the two-phase reaction mechanism. The test cells showed a discharge capacity of 137 and 155 mA h g^{-1} for CC and CC–CV modes, respectively. The obtained capacity through CC–CV mode is about ~91% of the theoretical capacity. The cycling profiles of Li/C–$LiMnPO_4$ cells with two different testing modes are presented in Fig. 12b. The capacity fading during cycling was noted for both test conditions and this fading was mainly because of Mn dissolution in electrolyte solutions.[108] The obtained values are in good agreement with the previous reports obtained by a solid-state approach. These results clearly suggested that the solid-state approach can also yield the high performance $LiMnPO_4$ particles after ball milling with an appropriate amount of carbon.

4 Summary and outlook

The present review highlights the various synthesis approaches that have been used to develop 4 V olivine phase $LiMnPO_4$ as a cathode material for Li-ion batteries. Among the synthesis routes reported in the literature and from our experience, the solid-state/polyol approach is found to be promising to yield a high performance olivine phase material by keeping bulk production in mind. For the case of native $LiMnPO_4$, irrespective of the synthesis routes employed, high energy ball milling is necessary to achieve a flat potential region at ~4.1 V *vs.* Li with high reversibility. Despite the size reduction of the particulates, it is not well understood why ball milling has been effectively utilized for $LiMnPO_4$. This clearly reflects the statement *Chemistry has its own secrets* by Tarascon and Armand.[13] Hence, the role of morphology in the drastic improvement in the electrochemical properties is not so dominant unlike $LiFePO_4$. However, some reports are available for nanostructured morphologies that exhibit very poor electrochemical profiles even when the applied current rate exceeds 0.5 C. This clearly reveals that there is not much scope in the shape controlled synthesis of $LiMnPO_4$, since during the ball milling procedure most of the shapes will be destroyed. In addition to the above, ball milling with a conductive additive, preferably carbon, yields a carbon coated $LiMnPO_4$ phase and such a coating certainly promotes conducting profiles, since the band gap of $LiMnPO_4$ lies in the insulator region (3.96 eV). Further, carbon content in the composite is such a crucial factor to increase the volumetric capacity; generally a carbon content of ~20 to 40% has been included during the ball milling procedure to achieve carbon coating. There is no doubt in this; inclusion of such a huge amount of carbon certainly provides an enhanced electronic conductivity of the composite. Nevertheless utilization of a huge carbon content dilutes the active material distribution and is subsequently detrimental to the volumetric capacity. Performance of the $LiMnPO_4$ phase is found to be better at elevated temperatures compared to ambient conditions, despite experiencing mild dissolution of Mn atoms in the electrolyte solution. However, the electrochemical performance at elevated temperatures is found to be better than the Mn based (~4 V *vs.* Li) spinel phase compound $LiMn_2O_4$. Apart from the conductive coatings, particle size and crystallization of the phase are also very crucial to achieve high rate performance. Though carbon coating alleviates the inherent nature of $LiMnPO_4$, still extraction of one mole Li from the lattice is found to be difficult. Therefore, a complex charging protocol, constant current–constant voltage (CC–CV mode, which is common in mobile chargers) mode is used for the extraction of one mole of Li. Another way to improve the electrochemical performance of the $LiMnPO_4$ phase is transition metal site doping (Mn sites with isovalent or aliovalent

substitutions) or Li-site doping. Both Mn and Li site doping provides improved battery performance irrespective of the testing temperature. The appearance of impurity traces during Li site doping is noted, particularly Li_3PO_4, which is an excellent ionic conductor and beneficial for the betterment of improved electrochemical performance at high rate operations. In Mn site substitution, Fe is found to be attractive (compared to Mg, Zn, Cu, Zr, V, Gd, Ti and Ni) and its concentration beyond 10% subsequently leads to the formation of a solid-solution between two olivine compounds ($LiMnPO_4$ and $LiFePO_4$). Substitution with Fe in Mn sites provides excellent electrochemical properties compared to the native compound, almost approaching the one mole Li extraction. The ball milling procedure may not be required for the case of the above solid-solutions. High performance olivine phase cathodes are obtained by varying the Fe concentration from 10 to 50%, but the reduction of the net operating potential and subsequent energy density has to be sacrificed in such solid-solutions. Similar to Fe, Cobalt also exhibits good solid-solution behavior with Mn, but the higher redox potential of Co^{2+} in the olivine phase prohibits its potential use. Hence, the development of a high voltage electrolyte is anticipated to realize the performance of Co based solid-solutions. Thermal stability is another very important criterion for a prospective electrode material in practical Li-ion batteries irrespective of the anode and cathode. It is well demonstrated that polyanion groups containing a phosphate matrix $(PO_4)^{3-}$ showed excellent thermal stability in both lithiated and delithiated states due to the strong covalent bond between oxygen and P^{5+} ions (P–O) compared to that of its oxide based counterparts ($LiCoO_2$, $LiMn_2O_4$, $Li(NiMnCo)_{1/3}O_2$, *etc.*). The thermal stability of $LiFePO_4$ is found to be exceptional in both charged and discharged states, whereas controversial reports are available for $LiMnPO_4$ and its derivatives including solid-solutions. Recently, Aurbach and co-workers[66] demonstrated excellent thermal stability of $LiMnPO_4$ and its solid-solutions (similar to $LiFePO_4$) which are not inferior to rest of the olivine phase or $(PO_4)^{3-}$ anion framework materials. Overall the highlight of this olivine phase $LiMnPO_4$ is that it is eco-friendly, cheap, thermally safe and has higher energy density (than $LiFePO_4$). Several challenges such as inherent electronic conductivity, size reduction and poor diffusion properties should be improved without compromising on the volumetric density to exploit in practical Li-ion cells. On the other hand, the solid-solution between Fe and Mn could be one of the better alternatives than both native compounds and can be used in high power applications like HEV and EV. The energy density of such solid-solutions lies between $\sim$580 and 700 W h kg^{-1} and depends on the choice of Fe concentration. However, still Mn dissolution will be a major problem for Mn based cathodes and it should be addressed for long term cyclability. A thin layer of surface coating with inert oxides (*e.g.* Al_2O_3, ZrO_2, TiO_2, *etc.*) by the ALD technique can be suggested to prevent the same.

Acknowledgements

V. Aravindan and S. Madhavi thank the National Research foundation (NRF, Singapore) for financial support through Competitive Research Programme (CRP) (grant no. NRF-CRP4-2008-03) and Clean Energy Research Project (CERP) (grant no. NRF-2009-EWT-CERP001-036). Y.S. Lee acknowledges the financial support from IT R&D program of MKE/KEIT. [KI10039182, Development of 5 V cathode material which capacity is 125 mAh g^{-1} & high voltage electrolyte which decomposition is over 5 V for lithium secondary battery.]

References

1 N.-S. Choi, Z. Chen, S. A. Freunberger, X. Ji, Y.-K. Sun, K. Amine, G. Yushin, L. F. Nazar, J. Cho and P. G. Bruce, *Angew. Chem., Int. Ed.*, 2012, **51**, 9994–10024.
2 J. B. Goodenough and Y. Kim, *Chem. Mater.*, 2009, **22**, 587–603.
3 V. Etacheri, R. Marom, R. Elazari, G. Salitra and D. Aurbach, *Energy Environ. Sci.*, 2011, **4**, 3243–3262.
4 O. K. Park, Y. Cho, S. Lee, H.-C. Yoo, H.-K. Song and J. Cho, *Energy Environ. Sci.*, 2011, **4**, 1621–1633.
5 B. Scrosati, J. Hassoun and Y.-K. Sun, *Energy Environ. Sci.*, 2011, **4**, 3287–3295.
6 V. Aravindan, J. Gnanaraj, S. Madhavi and H. K. Liu, *Chem.–Eur. J.*, 2011, **17**, 14326–14346.
7 A. Manthiram, *J. Phys. Chem. Lett.*, 2011, **2**, 176–184.
8 M. S. Whittingham, *Proc. IEEE*, 2012, **100**, 1518–1534.
9 E. J. Cairns and P. Albertus, *Annu. Rev. Chem. Biomol. Eng.*, 2010, **1**, 299–320.
10 C. M. Hayner, X. Zhao and H. H. Kung, *Annu. Rev. Chem. Biomol. Eng.*, 2012, **3**, 445–471.
11 G. L. Soloveichik, *Annu. Rev. Chem. Biomol. Eng.*, 2011, **2**, 503–527.
12 M. M. Thackeray, C. Wolverton and E. D. Isaacs, *Energy Environ. Sci.*, 2012, **5**, 7854–7863.
13 J. M. Tarascon and M. Armand, *Nature*, 2001, **414**, 359–367.
14 M. Armand and J. M. Tarascon, *Nature*, 2008, **451**, 652–657.
15 B. Xu, D. Qian, Z. Wang and Y. S. Meng, *Mater. Sci. Eng., R*, 2012, **73**, 51–65.
16 B. L. Ellis, K. Town and L. F. Nazar, *Electrochim. Acta*, 2012, **84**, 145–154.
17 A. Kraytsberg and Y. Ein-Eli, *Adv. Energy Mater.*, 2012, **2**, 922–939.
18 J. O. Besenhard and M. Winter, *ChemPhysChem*, 2002, **3**, 155–159.
19 M. S. Whittingham, *Science*, 1976, **192**, 1126–1127.
20 K. Mizushima, P. C. Jones, P. J. Wiseman and J. B. Goodenough, *Mater. Res. Bull.*, 1980, **15**, 783–789.
21 M. M. Thackeray, W. I. F. David, P. G. Bruce and J. B. Goodenough, *Mater. Res. Bull.*, 1983, **18**, 461–472.
22 J. Goodenough, *J. Solid State Electrochem.*, 2012, **16**, 2019–2029.
23 R. Yazami and P. Touzain, *J. Power Sources*, 1983, **9**, 365–371.
24 M. S. Whittingham, *Chem. Rev.*, 2004, **104**, 4271–4302.
25 P. Kalyani and N. Kalaiselvi, *Sci. Technol. Adv. Mater.*, 2005, **6**, 689.
26 M. M. Thackeray, S.-H. Kang, C. S. Johnson, J. T. Vaughey, R. Benedek and S. A. Hackney, *J. Mater. Chem.*, 2007, **17**, 3112–3125.

27 M. Park, X. Zhang, M. Chung, G. B. Less and A. M. Sastry, *J. Power Sources*, 2010, **195**, 7904–7929.
28 M. Winter, J. O. Besenhard, M. E. Spahr and P. Novák, *Adv. Mater.*, 1998, **10**, 725–763.
29 V. M. Elena, S. P. Vladislav and S. D. Valeriya, *Russ. Chem. Rev.*, 2004, **73**, 991.
30 P. Barpanda, S.-i. Nishimura and A. Yamada, *Adv. Energy Mater.*, 2012, **2**, 841–859.
31 A. Manthiram and J. B. Goodenough, *J. Power Sources*, 1989, **26**, 403–408.
32 A. Manthiram and J. B. Goodenough, *J. Solid State Chem.*, 1987, **71**, 349–360.
33 A. K. Padhi, K. S. Nanjundaswamy and J. B. Goodenough, *J. Electrochem. Soc.*, 1997, **144**, 1188–1194.
34 http://www.nedo.go.jp/content/100153964.pdf.
35 A. Manthiram, *Electrochem. Soc. Interface*, 2009, **18**, 44–47.
36 S.-T. Myung, K. Amine and Y.-K. Sun, *J. Mater. Chem.*, 2010, **20**, 7074–7095.
37 C. Li, H. P. Zhang, L. J. Fu, H. Liu, Y. P. Wu, E. Rahm, R. Holze and H. Q. Wu, *Electrochim. Acta*, 2006, **51**, 3872–3883.
38 H.-K. Song, K. T. Lee, M. G. Kim, L. F. Nazar and J. Cho, *Adv. Funct. Mater.*, 2010, **20**, 3818–3834.
39 N. A. Chernova, M. Roppolo, A. C. Dillon and M. S. Whittingham, *J. Mater. Chem.*, 2009, **19**, 2526–2552.
40 P. G. Balakrishnan, R. Ramesh and T. Prem Kumar, *J. Power Sources*, 2006, **155**, 401–414.
41 A. K. Padhi, K. S. Nanjundaswamy, C. Masquelier and J. B. Goodenough, *J. Electrochem. Soc.*, 1997, **144**, 2581–2586.
42 A. K. Padhi, K. S. Nanjundaswamy and J. B. Goodenough, *J. Electrochem. Soc.*, 1997, **144**, 1188–1194.
43 K. Zaghib, J. B. Goodenough, A. Mauger and C. Julien, *J. Power Sources*, 2009, **194**, 1021–1023.
44 C. Masquelier, A. K. Padhi, K. S. Nanjundaswamy and J. B. Goodenough, *J. Solid State Chem.*, 1998, **135**, 228–234.
45 A. K. Padhi, K. S. Nanjundaswamy, C. Masquelier, S. Okada and J. B. Goodenough, *J. Electrochem. Soc.*, 1997, **144**, 1609–1613.
46 K. S. Nanjundaswamy, A. K. Padhi, J. B. Goodenough, S. Okada, H. Ohtsuka, H. Arai and J. Yamaki, *Solid State Ionics*, 1996, **92**, 1–10.
47 J. B. Goodenough, *J. Power Sources*, 2007, **174**, 996–1000.
48 Z. Gong and Y. Yang, *Energy Environ. Sci.*, 2011, **4**, 3223–3242.
49 A. R. Cho, J. N. Son, V. Aravindan, H. Kim, K. S. Kang, W. S. Yoon, W. S. Kim and Y. S. Lee, *J. Mater. Chem.*, 2012, **22**, 6556–6560.
50 L.-X. Yuan, Z.-H. Wang, W.-X. Zhang, X.-L. Hu, J.-T. Chen, Y.-H. Huang and J. B. Goodenough, *Energy Environ. Sci.*, 2011, **4**, 269–284.
51 I. C. Jang, H. H. Lim, S. B. Lee, K. Karthikeyan, V. Aravindan, K. S. Kang, W. S. Yoon, W. I. Cho and Y. S. Lee, *J. Alloys Compd.*, 2010, **497**, 321–324.
52 I. C. Jang, C. G. Son, S. M. G. Yang, J. W. Lee, A. R. Cho, V. Aravindan, G. J. Park, K. S. Kang, W. S. Kim, W. I. Cho and Y. S. Lee, *J. Mater. Chem.*, 2011, **21**, 6510–6514.
53 L. Dimesso, C. Forster, W. Jaegermann, J. P. Khanderi, H. Tempel, A. Popp, J. Engstler, J. J. Schneider, A. Sarapulova, D. Mikhailova, L. A. Schmitt, S. Oswald and H. Ehrenberg, *Chem. Soc. Rev.*, 2012, **41**, 5068–5080.
54 W. F. Howard and R. M. Spotnitz, *J. Power Sources*, 2007, **165**, 887–891.
55 S. Okada, S. Sawa, M. Egashira, J.-i. Yamaki, M. Tabuchi, H. Kageyama, T. Konishi and A. Yoshino, *J. Power Sources*, 2001, **97–98**, 430–432.
56 A. Yamada, M. Hosoya, S. C. Chung, Y. Kudo, K. Hinokuma, K. Y. Liu and Y. Nishi, *J. Power Sources*, 2003, **119–121**, 232–238.
57 Z. X. Nie, C. Y. Ouyang, J. Z. Chen, Z. Y. Zhong, Y. L. Du, D. S. Liu, S. Q. Shi and M. S. Lei, *Solid State Commun.*, 2010, **150**, 40–44.
58 Y. Asari, Y. Suwa and T. Hamada, *Phys. Rev. B: Condens. Matter Mater. Phys.*, 2011, **84**, 134113.
59 G. Li, H. Azuma and M. Tohda, *Electrochem. Solid-State Lett.*, 2002, **5**, A135–A137.
60 S. W. Kim, J. Kim, H. Gwon and K. Kang, *J. Electrochem. Soc.*, 2009, **156**, A635–A638.
61 J. Kim, K.-Y. Park, I. Park, J.-K. Yoo, J. Hong and K. Kang, *J. Mater. Chem.*, 2012, **22**, 11964–11970.
62 J. Kim, K.-Y. Park, I. Park, J.-K. Yoo, D.-H. Seo, S.-W. Kim and K. Kang, *J. Electrochem. Soc.*, 2012, **159**, A55–A59.
63 C. Delacourt, P. Poizot, J.-M. Tarascon and C. Masquelier, *Nat. Mater.*, 2005, **4**, 254–260.
64 G. Chen and T. J. Richardson, *J. Power Sources*, 2010, **195**, 1221–1224.
65 S. P. Ong, A. Jain, G. Hautier, B. Kang and G. Ceder, *Electrochem. Commun.*, 2010, **12**, 427–430.
66 S. K. Martha, O. Haik, E. Zinigrad, I. Exnar, T. Drezen, J. H. Miners and D. Aurbach, *J. Electrochem. Soc.*, 2011, **158**, A1115–A1122.
67 S. P. Ong, A. Jain, G. Hautier, B. Kang and G. Ceder, *Electrochem. Commun.*, 2010, **12**, 427–430.
68 D. Choi, J. Xiao, Y. J. Choi, J. S. Hardy, M. Vijayakumar, M. S. Bhuvaneswari, J. Liu, W. Xu, W. Wang, Z. Yang, G. L. Graff and J.-G. Zhang, *EnergyEnviron. Sci.*, 2011, **4**, 4560–4566.
69 T. Shiratsuchi, S. Okada, T. Doi and J. i. Yamaki, *Electrochim. Acta*, 2009, **54**, 3145–3151.
70 S.-Y. Chung, J. T. Bloking and Y.-M. Chiang, *Nat. Mater.*, 2002, **1**, 123–128.
71 S. K. Martha, J. Grinblat, O. Haik, E. Zinigrad, T. Drezen, J. H. Miners, I. Exnar, A. Kay, B. Markovsky and D. Aurbach, *Angew. Chem., Int. Ed.*, 2009, **48**, 8559–8563.
72 D. Wang, H. Buqa, M. Crouzet, G. Deghenghi, T. Drezen, I. Exnar, N. H. Kwon, J. H. Miners, L. Poletto and M. Grätzel, *J. Power Sources*, 2009, **189**, 624–628.
73 S. K. Martha, O. Haik, V. Borgel, E. Zinigrad, I. Exnar, T. Drezen, J. H. Miners and D. Aurbach, *J. Electrochem. Soc.*, 2011, **158**, A790–A797.
74 Q.-Q. Zou, G.-N. Zhu and Y.-Y. Xia, *J. Power Sources*, 2012, **206**, 222–229.

75 C. G. Son, H. M. Yang, G. W. Lee, A. R. Cho, V. Aravindan, H. S. Kim, W. S. Kim and Y. S. Lee, *J. Alloys Compd.*, 2011, **509**, 1279–1284.
76 D. Wang, C. Ouyang, T. Dŕzen, I. Exnar, A. Kay, N. H. Kwon, P. Gouerec, J. H. Miners, M. Wang and M. Grätzel, *J. Electrochem. Soc.*, 2010, **157**, A225–A229.
77 J. W. Lee, M. S. Park, B. Anass, J. H. Park, M. S. Paik and S. G. Doo, *Electrochim. Acta*, 2010, **55**, 4162–4169.
78 B. Kang and G. Ceder, *J. Electrochem. Soc.*, 2010, **157**, A808–A811.
79 D. Choi, D. Wang, I.-T. Bae, J. Xiao, Z. Nie, W. Wang, V. V. Viswanathan, Y. J. Lee, J.-G. Zhang, G. L. Graff, Z. Yang and J. Liu, *Nano Lett.*, 2010, **10**, 2799–2805.
80 C. Hu, H. Yi, H. Fang, B. Yang, Y. Yao, W. Ma and Y. Dai, *Electrochem. Commun.*, 2010, **12**, 1784–1787.
81 H. Yi, C. Hu, H. Fang, B. Yang, Y. Yao, W. Ma and Y. Dai, *Electrochim. Acta*, 2011, **56**, 4052–4057.
82 Y. Wang, Y. Chen, S. Cheng and L. He, *Korean J. Chem. Eng.*, 2011, **28**, 964–968.
83 J. Hong, F. Wang, X. Wang and J. Graetz, *J. Power Sources*, 2011, **196**, 3659–3663.
84 B. Zhang, X. Wang, Z. Liu, H. Li and X. Huang, *J. Electrochem. Soc.*, 2010, **157**, A285–A288.
85 T. Muraliganth and A. Manthiram, *J. Phys. Chem. C*, 2010, **114**, 15530–15540.
86 J. Yang and J. J. Xu, *J. Electrochem. Soc.*, 2006, **153**, A716–A723.
87 N. H. Kwon, T. Drezen, I. Exnar, I. Teerlinck, M. Isono and M. Graetzel, *Electrochem. Solid-State Lett.*, 2006, **9**, A277–A280.
88 T. Drezen, N. H. Kwon, P. Bowen, I. Teerlinck, M. Isono and I. Exnar, *J. Power Sources*, 2007, **174**, 949–953.
89 T. Doi, S. Yatomi, T. Kida, S. Okada and J. I. Yamaki, *Cryst. Growth Des.*, 2009, **9**, 4990–4992.
90 G. Yang, H. Ni, H. Liu, P. Gao, H. Ji, S. Roy, J. Pinto and X. Jiang, *J. Power Sources*, 2011, **196**, 4747–4755.
91 J. K. Kim, C. R. Shin, J. H. Ahn, A. Matic and P. Jacobsson, *Electrochem. Commun.*, 2011, **13**, 1105–1108.
92 U. Dettlaff-Weglikowska, N. Sato, J. Yoshida and S. Roth, *Phys. Status Solidi B*, 2009, **246**, 2482–2485.
93 C. Nithya, R. Thirunakaran, A. Sivashanmugam and S. Gopukumar, *Chem.–Asian J.*, 2012, **7**, 163–168.
94 S. Moon, P. Muralidharan and D. K. Kim, *Ceram. Int.*, 2012, **38**, S471–S475.
95 T. R. Kim, D. H. Kim, H. W. Ryu, J. H. Moon, J. H. Lee, S. Boo and J. Kim, *J. Phys. Chem. Solids*, 2007, **68**, 1203–1206.
96 S. K. Martha, E. Markevich, V. Burgel, G. Salitra, E. Zinigrad, B. Markovsky, H. Sclar, Z. Pramovich, O. Heik, D. Aurbach, I. Exnar, H. Buqa, T. Drezen, G. Semrau, M. Schmidt, D. Kovacheva and N. Saliyski, *J. Power Sources*, 2009, **189**, 288–296.
97 S. K. Martha, B. Markovsky, J. Grinblat, Y. Gofer, O. Haik, E. Zinigrad, D. Aurbach, T. Drezen, D. Wang, G. Deghenghi and I. Exnar, *J. Electrochem. Soc.*, 2009, **156**, A541–A552.
98 M. Koltypin, D. Aurbach, L. Nazar and B. Ellis, *Electrochem. Solid-State Lett.*, 2007, **10**, A40–A44.
99 P. R. Kumar, M. Venkateswarlu, M. Misra, A. K. Mohanty and N. Satyanarayana, *J. Electrochem. Soc.*, 2011, **158**, A227–A230.
100 Z. Bakenov and I. Taniguchi, *Electrochem. Commun.*, 2010, **12**, 75–78.
101 Z. Bakenov and I. Taniguchi, *J. Power Sources*, 2010, **195**, 7445–7451.
102 Z. Bakenov and I. Taniguchi, *Mater. Res. Bull.*, 2011, **46**, 1311–1314.
103 T. N. L. Doan, Z. Bakenov and I. Taniguchi, *Adv. Powder Technol.*, 2010, **21**, 187–196.
104 T. N. L. Doan and I. Taniguchi, *J. Power Sources*, 2011, **196**, 1399–1408.
105 I. Taniguchi, T. N. L. Doan and B. Shao, *Electrochim. Acta*, 2011, **56**, 7680–7685.
106 S. M. Oh, H. G. Jung, C. S. Yoon, S. T. Myung, Z. Chen, K. Amine and Y. K. Sun, *J. Power Sources*, 2011, **196**, 6924–6928.
107 S. M. Oh, S. W. Oh, S. T. Myung, S. M. Lee and Y. K. Sun, *J. Alloys Compd.*, 2010, **506**, 372–376.
108 S. M. Oh, S. W. Oh, C. S. Yoon, B. Scrosati, K. Amine and Y. K. Sun, *Adv. Funct. Mater.*, 2010, **20**, 3260–3265.
109 C. Delacourt, L. Laffont, R. Bouchet, C. Wurm, J. B. Leriche, M. Morcrette, J. M. Tarascon and C. Masquelier, *J. Electrochem. Soc.*, 2005, **152**, A913–A921.
110 C. Delacourt, P. Poizot, M. Morcrette, J. M. Tarascon and C. Masquelier, *Chem. Mater.*, 2004, **16**, 93–99.
111 C. Delacourt, C. Wurm, P. Reale, M. Morcrette and C. Masquelier, *Solid State Ionics*, 2004, **173**, 113–118.
112 J. Xiao, W. Xu, D. Choi and J. G. Zhang, *J. Electrochem. Soc.*, 2010, **157**, A142–A147.
113 J. Xiao, N. A. Chernova, S. Upreti, X. Chen, Z. Li, Z. Deng, D. Choi, W. Xu, Z. Nie, G. L. Graff, J. Liu, M. S. Whittingham and J.-G. Zhang, *Phys. Chem. Chem. Phys.*, 2011, **13**, 18099–18106.
114 D.-K. Kim, H.-M. Park, S.-J. Jung, Y. U. Jeong, J.-H. Lee and J.-J. Kim, *J. Power Sources*, 2006, **159**, 237–240.
115 S. B. Lee, S. H. Cho, J. B. Heo, V. Aravindan, H. S. Kim and Y. S. Lee, *J. Alloys Compd.*, 2009, **488**, 380–385.
116 J. Ma and Q. Z. Qin, *J. Power Sources*, 2005, **148**, 66–71.
117 S.-M. Oh, S.-T. Myung, Y. S. Choi, K. H. Oh and Y.-K. Sun, *J. Mater. Chem.*, 2011, **21**, 19368–19374.
118 Y.-K. Sun, S.-M. Oh, H.-K. Park and B. Scrosati, *Adv. Mater.*, 2011, **23**, 5050–5054.
119 S.-M. Oh, S.-T. Myung, J. B. Park, B. Scrosati, K. Amine and Y.-K. Sun, *Angew. Chem., Int. Ed.*, 2012, **51**, 1853–1856.
120 H. Fang, L. Li and G. Li, *Chem. Lett.*, 2007, 436–437.
121 H. Fang, L. Li, Y. Yang, G. Yan and G. Li, *Chem. Commun.*, 2008, 1118–1120.
122 G. Chen, J. D. Wilcox and T. J. Richardson, *Electrochem. Solid-State Lett.*, 2008, **11**, A190–A194.
123 Y. Wang, Y. Yang and H. Shao, *Mater. Res. Bull.*, 2009, **44**, 2139–2142.
124 Y. Wang, Y. Yang and H. Shao, *Solid State Commun.*, 2010, **150**, 81–85.
125 K. Saravanan, J. J. Vittal, M. V. Reddy, B. V. R. Chowdari and P. Balaya, *J. Solid State Electrochem.*, 2010, **14**, 1755–1760.

126 K. Saravanan, V. Ramar, P. Balaya and J. J. Vittal, *J. Mater. Chem.*, 2011, **21**, 14925–14935.
127 G. R. Gardiner and M. S. Islam, *Chem. Mater.*, 2009, **22**, 1242–1248.
128 P. Nie, L. Shen, F. Zhang, L. Chen, H. Deng and X. Zhang, *CrystEngComm*, 2012, **14**, 4284–4288.
129 A. Manthiram, A. Vadivel Murugan, A. Sarkar and T. Muraliganth, *Energy Environ. Sci.*, 2008, **1**, 621–638.
130 A. Vadivel Murugan, T. Muraliganth, P. J. Ferreira and A. Manthiram, *Inorg. Chem.*, 2009, **48**, 946–952.
131 A. Vadivel Murugan, T. Muraliganth and A. Manthiram, *J. Electrochem. Soc.*, 2009, **156**, A79–A83.
132 H. Ji, G. Yang, H. Ni, S. Roy, J. Pinto and X. Jiang, *Electrochim. Acta*, 2011, **56**, 3093–3100.
133 G. Chen, A. K. Shukla, X. Song and T. J. Richardson, *J. Mater. Chem.*, 2011, **21**, 10126–10133.
134 T. Li, T. Mei, Y. Zhu, H. Gong, T. Huang and Y. Qian, *Chem. Lett.*, 2011, 837–839.
135 J. Ni and L. Gao, *J. Power Sources*, 2011, **196**, 6498–6501.
136 J. Ni, Y. Kawabe, M. Morishita, M. Watada and T. Sakai, *J. Power Sources*, 2011, **196**, 8104–8109.
137 F. Wang, J. Yang, P. Gao, Y. NuLi and J. Wang, *J. Power Sources*, 2011, **196**, 10258–10262.
138 K. Dokko, T. Hachida and M. Watanabe, *J. Electrochem. Soc.*, 2011, **158**, A1275–A1281.
139 H. Wang, Y. Yang, Y. Liang, L.-F. Cui, H. Sanchez Casalongue, Y. Li, G. Hong, Y. Cui and H. Dai, *Angew. Chem., Int. Ed.*, 2011, **50**, 7364–7368.
140 P. Barpanda, K. Djellab, N. Recham, M. Armand and J. M. Tarascon, *J. Mater. Chem.*, 2011, **21**, 10143–10152.
141 H. Yoo, M. Jo, B.-S. Jin, H.-S. Kim and J. Cho, *Adv. Energy Mater.*, 2011, **1**, 347–351.
142 D. Rangappa, K. Sone, Y. Zhou, T. Kudo and I. Honma, *J. Mater. Chem.*, 2011, **21**, 15813–15818.
143 M. K. Devaraju and I. Honma, *Adv. Energy Mater.*, 2012, **2**, 284–297.
144 S. Geller and J. L. Durand, *Acta Crystallogr.*, 1960, **13**, 325–331.